Since January 2020 Elsevier has created a COVID-19 resource centre with free information in English and Mandarin on the novel coronavirus COVID-19. The COVID-19 resource centre is hosted on Elsevier Connect, the company's public news and information website.

Elsevier hereby grants permission to make all its COVID-19-related research that is available on the COVID-19 resource centre - including this research content - immediately available in PubMed Central and other publicly funded repositories, such as the WHO COVID database with rights for unrestricted research re-use and analyses in any form or by any means with acknowledgement of the original source. These permissions are granted for free by Elsevier for as long as the COVID-19 resource centre remains active.

Current Research in Chemical Biology 2 (2022) 100021

Contents lists available at ScienceDirect

Current Research in Chemical Biology

journal homepage: www.journals.elsevier.com/current-research-in-chemical-biology

Recent advances on therapeutic potentials of gold and silver nanobiomaterials for human viral diseases

Yusuf Oloruntoyin Ayipo [a,b,*], Ajibola Abdulahi Bakare [c], Umar Muhammad Badeggi [d,e], Akeem Adebayo Jimoh [b], Amudat Lawal [f], Mohd Nizam Mordi [a]

[a] Centre for Drug Research, Universiti Sains Malaysia, 11800, Pulau Pinang, Malaysia
[b] Department of Chemistry and Industrial Chemistry, Kwara State University, Malete, P. M. B. 1530, Ilorin 240001, Nigeria
[c] Department of Materials and Environmental Technology, Tallinn University of Technology, Ehitajate tee 5, 19086 Tallinn, Estonia
[d] Department of Chemistry, Ibrahim Badamasi Babangida University Lapai, P. M. B. 11, Minna 4947, Nigeria
[e] Department of Chemistry, Cape Peninsula University of Technology, Symphony Rd., Bellville 7535, South Africa
[f] Department of Chemistry, University of Ilorin, P. M. B. 1515, Ilorin, Nigeria

ARTICLE INFO

Keywords:
Nanobiomaterials
Viral diseases
Gold and silver
Bioorganic and bioinorganic synthesis
Next-generation antiviral therapeutics

ABSTRACT

Viral diseases are prominent among the widely spread infections threatening human well-being. Real-life clinical successes of the few available therapeutics are challenged by pathogenic resistance and suboptimal delivery to target sites. Nanotechnology has aided the design of functionalised and non-functionalised Au and Ag nanobiomaterials through physical, chemical and biological (green synthesis) methods with improved antiviral efficacy and delivery. In this review, innovative designs as well as interesting antiviral activities of the nanotechnology-inclined biomaterials of Au and Ag, reported in the last 5 years were critically overviewed against several viral diseases affecting man. These include influenza, respiratory syncytial, adenovirus, severe acute respiratory syndromes (SARS), rotavirus, norovirus, measles, chikungunya, HIV, herpes simplex virus, dengue, polio, enterovirus and rift valley fever virus. Notably identified among the nanotechnologically designed promising antiviral agents include **AuNP-M2e peptide vaccine**, **AgNP of cinnamon bark extract** and **AgNP of oseltamivir** for influenza, **PVP coated AgNP** for RSV, **PVP-AgNPs** for SARS-CoV-2, **AuNRs** of a **peptide pregnancy-induced hypertension** and **AuNP nanocarriers** of **antigen** for MERS-CoV and SARS-CoV respectively. Others are **AgNPs of collagen and *Bacillus subtilis*** for rotavirus, **AgNPs labelled Ag30–SiO_2** for murine norovirus in water, **AuNPs** of ***Allium sativum*** and **AgNPs** of **ribavirin** for measles, **AgNPs of *Citrus limetta*** and ***Andrographis Paniculata*** for Chikungunya, **AuNPs** of **efavirenz** and **stavudine**, and **AgNPs-curcumin** for HIV, **NPAuG3-S8** for HSV, **AgNPs of *Moringa oleifera*** and ***Bruguiera cylindrica*** for dengue while **AgNPs** of **polyethyleneimine** and **siRNA** analogues displayed potency against enterovirus. The highlighted candidates are recommended for further translational studies towards antiviral therapeutic designs.

1. Introduction

Viruses are the smallest microbes proven to be of great threat to human well-being with no known cure for a high number of their taxonomical strains (García-Serradilla et al., 2019; Draz and Shafiee, 2018). They are responsible for most human pathogenic infections and are difficult to manage for health practitioners. Several viruses such as influenza, hepatitis, Ebola, Zika virus, human immunodeficiency virus (HIV), herpes simplex virus (HSV), Hepatitis C virus (HCV) and recently coronaviruses (CoVs) have been identified as a serious threat to humanity through disease outbreaks and pandemics (Akbarzadeh et al., 2018; Ellah et al., 2019). For instance, the coronavirus 2019 (COVID-19) pandemic overwhelmed the world healthcare and economic systems, infecting millions of people, with a higher mortality rate amongst the vulnerable. Governments and health bodies across the globe had to devise various effective strategies to prevent the spread of the virus, which remains a big struggle. Till this moment, scientific efforts are being made by researchers to find a vaccine and effective treatment options for the infection with limited success (Palmieri and Papi, 2020). Generally, despite the enormous efficacious potentials of some topical virucidal agents, toxicity, the resistance of the pathogens and suboptimal delivery of the agents to target sites contributively limit their real-life clinical

* Corresponding author. Centre for Drug Research, Universiti Sains Malaysia, 11800, Pulau Pinang, Malaysia.
E-mail address: yusuf.ayipo@kwasu.edu.ng (Y.O. Ayipo).

https://doi.org/10.1016/j.crchbi.2022.100021
2666-2469/© 2022 The Author(s). Published by Elsevier B.V. This is an open access article under the CC BY-NC-ND license (http://creativecommons.org/licenses/by-nc-nd/4.0/).

successes (Malik et al., 2018; Parboosing et al., 2018). These make the treatment of viral diseases remain a challenging task.

Among the strategies for mitigating the limitations, the application of nanotechnology through further modifications of active biomaterials into functionalised and non-functionalised nanoparticles (NPs) facilitate the designs of nano-biomaterials with promising advantages over larger particles in terms of efficacy, enhanced delivery to targets, safety, cost-effectiveness and environmental friendliness (Choudhary et al., 2020; El-Sheekh et al., 2020). The functionalised types are usually comprising organic-based NPs or organic-capped analogues of metals such as Ag, Au, Pt, Fe, Cu and Zn with antiviral effects traceable to ligand-receptor chemical interactions while the non-functionalised counterparts are mostly pure inorganic materials such as the NPs of SiO_2, ZnO, $CuCl_2$, TiO_2 and CeO_2 (Lysenko et al., 2018; Sharma et al., 2019; Singh et al., 2019; Tamil Selvan et al., 2019). The nano-sized biomaterials have been designed through various techniques including physical, chemical and biological (i.e. algae, fungi and bacteria) with advantages of morphologies, favouring pharmacokinetics at target sites (El-Sheekh et al., 2020). Consequently, some formulated gold-based nanobiomaterials with *in vivo* activities have been recently overviewed and suggested for the development of antibodies against bacterial, parasitic and viral infection upon further study (Dykman, 2020). Similarly, based on their interesting performances in experimental models, few others are suggestively worthy of exploration as potential adjuvant/stand-alone vaccines against the dengue virus (Quach et al., 2018), foot and mouth disease (Teng et al., 2018), rift valley fever (Soliman et al., 2017), HIV (Gianvincenzo et al., 2015) and respiratory syncytial virus (Stone et al., 2013).

Nanotechnology has been gaining a great deal of scientific attention as a means of delivering medicinally attractive NPs with promising performances associated with synthetic accessibility, solubility, stability, release pattern and cell penetration, and uptake (Ellah et al., 2019). The Au and Ag NPs have been documented with effective potentials for the prevention, diagnosis, treatment and mitigation of the spread of several virulent viral diseases including the HIV, HSV, HCV, severe acute respiratory syndrome CoV 1 (SARS-CoV-1), Middle East respiratory syndrome CoV (MERS-CoV) and the recent SARS-CoV-2 pandemic. They demonstrate multi-mechanisms of actions such as photothermal effects, photocatalysis, intercalation/inhibition of viral DNA/RNA, apoptotic-inclined interactions and disruptive mimicry of viral structures due to morphological similarities. Other emerging feature-dependent medical and biomedical advantages of the NPs include drug delivery, biosensing, disinfection, bioimaging, point-of-care devices for biomolecule detection, cellular disruption, immunotherapy and antimicrobial efficacy (Campos et al., 2020; Weiss et al., 2020; Medhi et al., 2020; Tram et al., 2016; Talebian et al., 2020; Rodriguez-Izquierdo et al., 2020). Moreover, the technology steadily features various scientific and allied disciplines including biology, chemistry, medicine, engineering, computational and material sciences as an integral part of modern interdisciplinary sciences (Javaid et al., 2018). Although, few of the recently documented literature reflects the biomedical potentials of some topical NPs (Yaqoob et al., 2020; Murphy et al., 2015; Maduray and Parboosing, 2020; Ratan et al., 2021), while some were focused on antiviral potentials of nanoparticles generally without specificity on Au and Ag NPs (Fawzy et al., 2021; Kumari and Chatterjee, 2021; Li et al., 2021). Additionally, Babaei and co-researchers also reported an overview of antiviral activities of AuNPs experimented *in vitro* (Babaei et al., 2021), with less focus on AgNPs and their performances *in vivo,* where physiological side effects could be critically observed. However, the extensive coverage of the convenient methods of the nanotechnological designs of the nanobiomaterials of Au and Ag and their interesting efficacy specifically over a broad spectrum of human viral diseases remain underscored. In this review, innovative designs, as well as interesting antiviral activities of the nanotechnology-inclined biomaterials of Au and Ag, reported in the last 5 years were critically overviewed with more attention on synthetic accessibility and promising efficacy against several viral diseases affecting man.

2. Synthesis and characterization of metal nanoparticles

Although there are several methods through which metal nanoparticles (MNPs) such as Au and Ag NPs are synthesized, these are categorized basically into three main groups as physical, chemical and biological methods (Khan et al., 2018). The physical methods such as sonochemical and laser ablation use the top-down approach and mostly produce monodispersed NPs. Unfortunately, so much waste is generated in addition to the required sophisticated resources. These limit their use, especially for certain biomedical applications (Parboosing et al., 2018).

The chemical method such as hydrothermal synthesis, on the other hand, uses the bottom-up approach, leading to the production of NPs of well-defined dimensions, structures and sizes. In this approach, metal ions such as those of Au and Ag are reduced by reducing agents. The reductants could be organic or inorganic agents. Often, stabilizing agents such as organic solvents, synthetic or natural polymers are employed to prevent the NPs from aggregation. Alternatively, surfactants containing specific functionalities (e.g. nitrogen and oxygen-containing groups) have also acted as stabilizers, protecting the NPs from agglomeration or sedimentation. Comparatively to the physical methods, these techniques are more fascinating and economical. Despite these qualities, the chemical methods may not be without some disadvantages such as environmental pollution due to the toxic nature of the chemicals that might have been employed. Hence, some of the NPs from this route may not be suitable for certain biomedical applications (Parboosing et al., 2018).

The biological method also known as the green synthesis depends on the bottom-up approach, employing unicellular and extracellular biological organisms (e.g. bacteria, algae and plants). This technique is relatively simple, cost-effective and environmentally friendly. Biogenic NPs are biocompatible, easily scalable to large quantities, eco-friendly, however, challenged with size and shape moderation. Several factors such as pH, temperature, type, concentration of the reducing agent and synthesis time among others influence their size, morphology and stability. The NPs synthesized through the green (biological) method are relatively safer and associated with fewer toxic by-products (Ijaz et al., 2020), making them more preferable for biomedical applications. The extract of several plants parts such as leaves, roots, stem bark, flowers and seeds have been used in the fabrication of both metal NPs. For instance, *Citrus limetta* peels (Choudhary et al., 2020), aqueous extract of *Cinnamon cassia* (Fatima et al., 2015), *Allium sativum* (Meléndez-Villanueva et al., 2019), *Pelargonium sidoides* (Badeggi et al., 2020a), *Leucosidea sericea* (procyanidins) (Badeggi et al., 2020b, 2020c) have been used for the biological synthesis of both Au and Ag NPs. Additionally, the green synthesis entails the use of microorganisms such as bacteria, fungi, and viruses for producing metal NPs of immense biological functions. There are numerous advantages in the use of biological methods, considering biocompatibility, safety to the environment, easy production in addition to avoiding carcinogenicity and cytotoxicity. Thus, biological methods are more preferred to physical and chemical methods.

Another important aspect of the preparation of MNPs is the determination of their physicochemical properties. Understanding the characteristic features such as size, shape, surface charge, morphology and distribution are of utmost importance as most applications are dependent on the parameters (Lakshminarayanan et al., 2018). The ultra-violet visible (UV–Vis) spectroscopy, transmission electron microscopy (TEM), selected area electron diffraction (SAED), X-ray diffraction (XRD), dynamic light scattering (DLS), energy dispersive X-ray (EDX) spectroscopy are among the commonly applied techniques to determine absorbance, size and morphology, crystallinity, polydispersity, hydrodynamic size, and zeta potential (ZP) of MNPs (Ahmad et al., 2019; Khoobchandani et al., 2020; Abdulla et al., 2020; Ibrahim et al., 2021). The surface plasmon resonance (SPR) of NPs may depend on the metal involved among other factors. For instance, while AgNPs possess SPR at about 320–500 nm, the Au counterparts appear at 500–600 nm (Weiss et al., 2020). From the TEM micrographs, the morphology and size of the MNPs

can be determined. Although usually bigger than that measured by the TEM analysis, the DLS measurement also provides information on the size alongside the polydispersity index (PDI), used to determine the degree of homogeneity of the particles in colloidal solutions (Danaei et al., 2018). The ZP shows the extent of stability of the colloidal solutions. The ZP values could be positive or negative depending on the type of ions surrounding the surface of the NPs. However, the degree of stability is dependent on the magnitude of the ZP value and not the charge (Danaei et al., 2018). Several studies have employed XRD in conjunction with SAED to confirm the crystallinity of MNPs (Vijilvani et al., 2019). The EDX has been used to further confirm the type of MNPs that has been synthesized since it can detect heavy metals such as Au and Ag (Govindappa et al., 2018).

3. Synthesis and characterization of gold nanoparticles

3.1. Chemical method

Chloroauric acid was reduced by trisodium citrate ($Na_3C_6H_5O_7.2H_2O$) to synthesize AuNPs using the Turkevich method. The synthesised NPs were characterised using UV–Vis spectroscopy, then PEGylated and subjected to a colloidal stability test. The PEGylated AuNPs were reacted with linker N-succinimidyl 3-(2-pyridyldithio) propionate molecule, while the subsequent product was conjugated with RNA before being coated with polyethyleneimine. Size, polydispersity, concentration and ZP of the NPs were tested for at the end of each synthesis step. The characterization results indicated mean core diameters of the NPs between 30 and 40 nm, λ_{max} 527–530 nm and ZPs in the range of −21.4 and 13.5 mV (Parboosing et al., 2018). Malik et al. reportedly prepared Efaverinz and AuNPs loaded niosomes by employing the reverse phase evaporation technique. The loaded niosomes were characterized, giving a PDI of 0.276 and an average particle size of 10.4 nm. The particles were spherical with a ZP of 2.54 mV and UV–Vis maximum absorption at 530 nm. The O-palmitoylmannan (OPM) was successfully synthesized by the esterification process from mannose, and the FTIR characterization indicated the participation of mannan CH_2OH in the esterification process. The synthesized OPM and Efaverinz-AuNPs loaded niosomes were incubated for 12h at 32 °C while gel chromatography was used for purification. The synthesized OPM anchored Efaverinz-AuNPs loaded niosomes were further observed with PDI of 0.326, hydrodynamic size of 892.3 nm and a significantly reduced ZP as −52.50 mV (Malik et al., 2018).

Some AuNPs of Ribavirin were prepared by dissolving Ribavirin powder ($C_8H_{12}N_4O_5$) in AuNP. The suspension was kept in a dark bottle and shaken for 24 h at 37 °C. The AuNP-Ribavirin was separated from the excess ribavirin using centrifugation and washed with phosphate buffer saline. The characterization results indicated that 39.8% (199 μg/mL) of ribavirin was loaded onto the AuNP. Both AuNP and AuNP-Ribavirin showed an average diameter of 15 nm with respective ZP of −38 and −30.3 mV while the presence of Au in the nanocomposites was indicated by UV–Vis λ_{max} of 525 nm (Ahmed et al., 2018). Acyclovir was dispersed in an equimolar amount of (sulfobutyl ether-β-cyclodextrin) SBE-β-CD-containing water, stirred at room temperature for 24 h. The mixture was filtered on reaching equilibrium and the filtrate freeze-dried for 16 h. The drug-loaded nanodroplets were formed by dissolving the freeze-dried ACV-SBE-β-CD inclusion complex in distilled water, followed by the addition of chitosan nanodroplets under magnetic stirring. The resulting nanodroplets were characterized with FTIR spectroscopy indicating the participation of ACV functional groups, an average diameter of 400 nm, while their PDI and ZP were recorded as 0.20 and 19.98 mV respectively (Donalisio et al., 2020). Gold NP capped with citrate was synthesized by the citrate reduction method of chloroauric acid. Chloroauric acid was heated to boiling and stirred with prepared citrate solution added quickly leading to a change of colour from yellow to colourless and finally to deep red showing the formation of AuNP. The resulting solution was left to cool to room temperature. PEGlation of the citrated AuNP was done after the solution turned purple at the end of PEGlation. The redshift in UV–Vis λ_{max} (from 520 to 529 nm) between the citrated and PEGlated AuNPs supported a successful PEGlation. The TEM image indicated the particle size of ≈12 and ≈ 15 nm for citrated and PEGlated AuNPs while their respective ZPs were recorded as −12.3 and −38 mV (El-Gaffary et al., 2019).

3.2. Biological method

Chloroauric acid was added to *Oscillatoria* sp. and *Spirulina platensis* respectively to biosynthesize AuNPs of the respective algae. It was observed during the biosynthesis of the NPs that the microalgae could either produce NPs extracellularly or reduce the metallic ions intracellularly. Mechanical mashing for 1h at room temperature was applied to disrupt the cells to enable the release of the NPs into the aqueous solution. The separated AuNPs were washed and dried at 50 °C. The characterization results of FTIR confirmed the participation of the functional groups of the polysaccharides and proteins in the capping, reducing and stabilization of the NPs. The TEM image showed the NP shapes as octahedral, pentagonal and triangular with a size range of 15.60–77.13 nm (El-Sheekh et al., 2020). Some AuNPs of peptide nucleic acid (PNA) were prepared by mixing AuNPs with PNA, stabilized with the addition of 50 μL of fetal bovine serum (FBS). The characterization of AuNPs and AuNP-PNA was achieved with ZP recorded as −19.9 and −10.2 mV, UV–Vis spectra shift from 520 to 560 nm respectively and TEM indicating the average diameter of the synthesised NPs as 13 nm (Ghaffari et al., 2019). Mehranfar and co-workers recently reported the design of functionalised AuNPs of 8-mercaptooctan-1-aminium (Amin), 3-mercapto-ethyl sulfonate (Mes), 2-(2-(6-mercaptohexyl)oxy)ethoxy)ethan-1-ol (EG2), octane thiol (Ot), undecanesulfonic acid (Mus), Mus/Ot and a new peptide (Pep) consisting of 15 amino acid residues from human angiotensin-converting enzyme 2 (ACE2) active site with proposed structures (Fig. 1). The materials were theoretically investigated for inhibitory potentials against SARS-CoV-2 entry through the RNA binding domain (RBD) of spike glycoprotein, although with a limited report on characterization (Mehranfar and Izadyar, 2020).

Prepared extract of garlic (*A. sativum*) and chloroauric acid ($HAuCl_4$) were used to synthesize AuNP following the Turkevich method. The NPs were purified through a 0.2 μm filter, characterized with SPR at 537 nm, the average size of 6 nm, ZP of 21.2 mV while the TEM image indicated spherical shapes (Meléndez-Villanueva et al., 2019). Two types of AuNPs were synthesized and coupled with silica. They were annotated as type "a" which was a sol-gel and a powdered type "b" with different diameters at 12–30 nm and 50–200 nm respectively and consequently, varied activity against adenoviruses (Lysenko et al., 2018). Series of AuNPs, annotated as NPAuG1-S2, NPAuG2-S3 and NPAuG3-S8 with differing generation numbers 1–3 and some charge numbers of 2, 4 and 8 respectively were prepared. Although little was reported about their characterization, however, their impressive activity in cancer, cellular disruption and immunotherapy inspired the evaluation against the herpes simplex virus (Rodriguez-Izquierdo et al., 2020).

Gold NPs of stavudine was obtained by mixing AuNPs with stavudine solution, incubated with shaking for 24 h at room temperature. The successful coupling of stavudine with AuNPs to form composites was confirmed with a change in UV–Vis λ_{max} from 265 to 532 nm and variations in ZPs as −51.63, 66.70 and −5.00 mV for the AuNPs of citrate, polyethene imine (PEI) and polyethene glycol (PEG) respectively at 40 nm size (Zazo et al., 2017). A vaccine formulation was developed by Tao et al. comprising of ion channel membrane matrix protein 2 (M2e) coupled with AuNPs, with sCpG acting as a soluble adjuvant, taking advantage of interesting gold-thiol chemistry which aided the conjugation. Although little was reported of the characterization of the antibody, however, its immunogenicity significantly improved upon formulation into AuNP-M2e+sCpG (Tao et al., 2017). Two AuNPs conjugates (AuNP+ Hex and AuNP+Hex+Tat) were synthesized using a coupling reaction to link hexapeptide and Tat peptide to the surface of the AuNPs.

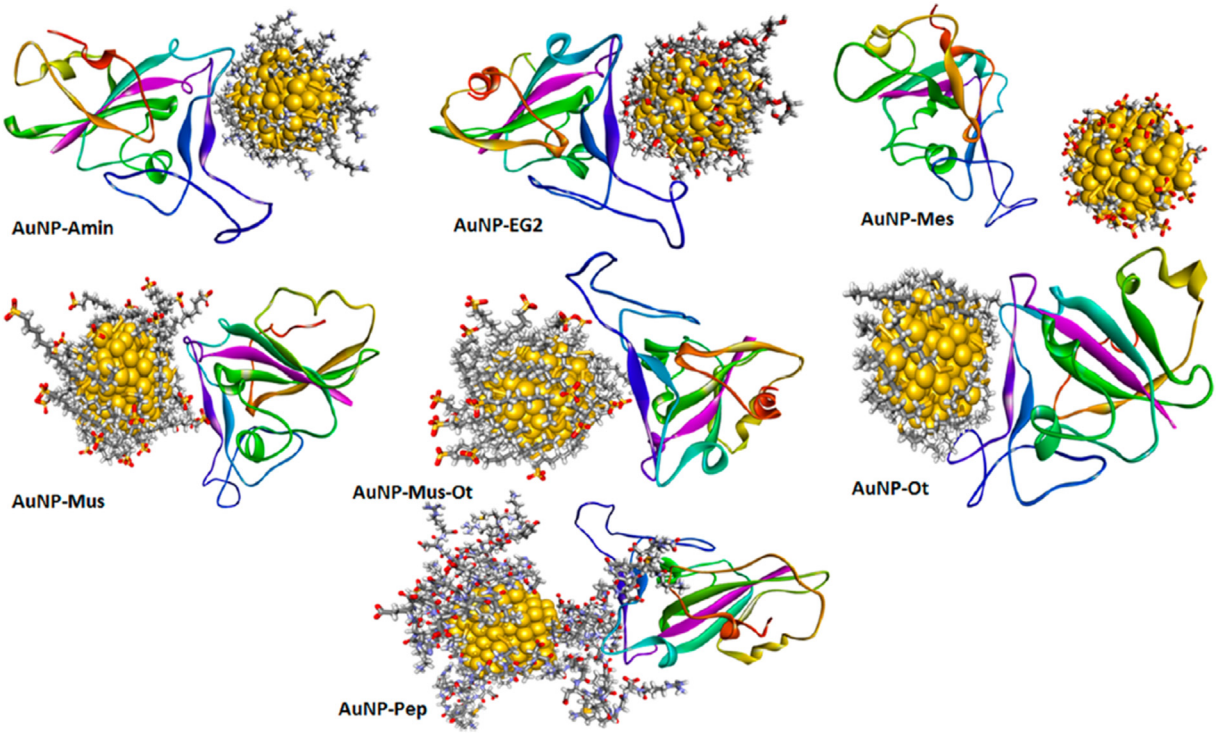

Fig. 1. Structures of RBD complexes with different functionalised AuNPs after simulation. (Reprinted with permission from (Mehranfar and Izadyar, 2020), copyright (2020) American Chemical Society).

The AuNP and its corresponding formulated product, AuNP+Hex+Tat showed UV–Vis λ_{max} of 500–600 nm, indicating the presence of Au and change in absorbance due to NP formation. They were further characterised, depicting sizes of 37.4 and 49.2 nm, and ZP of −22.9 and −13.7 mV respectively (Singh et al., 2019). Flupep ligand was used to functionalize AuNPs by adding the ligand mixture to AuNPs. The resultant NPs were observed under UV–Vis with maximum absorption at 520 nm while their average diameter was recorded as 10 nm. It was explored as a delivery system for Flupep and increased antiviral activity (Alghrair et al., 2019). Other synthesized AuNPs of interesting alkaloids such as the β-carboline and their extracts were not overviewed due to their reported off-scope applications as anticancer and antibacterial, though, the alkaloids possess antiviral potentials (Vo et al., 2019; Wu et al., 2017). Nevertheless, the alkaloids have been documented with interesting pharmacology as antiviral and anticancer, vast in natural products and possess good synthetic accessibility and bioavailability

Table 1
Physicochemical properties of gold nanoparticles with antiviral potentials.

Precursor materials	Method of synthesis	Colour	λ_{max} (nm)	Size/shape of NPs	Zeta potential	Polydispersity index	References
Ribavirin, chloroauric acid, sodium citrate dihydrate	Chemical	AuNPs: wine red AuNPs of ribavirin: blue	AuNPs- 525 AuNPs of ribavirin- 650	AuNPs: 15 nm AuNPs of ribavirin: 28.65nm/ Spherical	AuNPs: −38 mV AuNPs of ribavirin: −30.3 mV	NA	Ahmed et al. (2018)
Acyclovir, SBE-β-CD, chitosan nanodroplets	Chemical	NA	NA	395.4 nm/ Spherical	19.98 mV	0.20	Donalisio et al. (2020)
Thiol-containing polyethene glycol, tri-sodium citrate, hydrogen tetra-chloroaurate-trihydrate	Chemical	Citrated AuNPs: Deep red PEGlated AuNPs: light purple	Citrated AuNPs: 520 PEGlated AuNPs: 529	Citrated AuNPs: 12 nm PEGlated AuNPs: 15 nm/Spherical	Citrated AuNPs: −12.3 mV PEGlated AuNPs: −38 mV	NA	El-Gaffary et al. (2019)
Spirulina platensis and *Oscillatoria* sp.	Biological	Purple	552	15.60–77.13 nm/Octahedral, pentagonal and triangular	NA	NA	El-Sheekh et al. (2020)
Peptide nucleic acid	Chemical	Red	AuNPs: 520 PNA-AuNPs:560	13 nm	AuNPs: −19.5 mV PNA-AuNPs: −10.2 mV	NA	Ghaffari et al. (2019)
Allium sativa	Biological	Red	537	6 nm	+21.2 mV	NA	Meléndez-Villanueva et al. (2019)
Trisodium citrate, chloroauric acid	Chemical	Wine red	527–533	30–78.1 nm	−21.4 mV–13.5 mV	NA	Parboosing et al. (2018)

NA: Not available/not reported.

(Ayipo et al., 2021a, 2021b), worthy of exploration through the design into NPs. The biological method represents the most explored for the design of the NPs possibly due to its cost-effectiveness, convenient synthetic approach and safety to the environment. The summary of the synthetic method and physicochemical properties of the overviewed AuNPs is presented in Table 1.

4. Synthesis and characterization of silver nanoparticles

4.1. Physical method

Using the sonochemical method, Ag nanorods of sodium 2-mercaptoethane sulfonate (MES) were synthesized. Scanning electron microscopy (SEM) was used to determine the molecular size and morphology of the nanorods while FTIR spectra showed the presence of the nanorods conjugation between 400 and 4000 cm^{-1}. The spectra peak at 2571 cm^{-1} attributed to the S–H stretch supported the attachment of MES to AgNPs. The quantity of sodium 2-mercaptoethane sulfonate on the surface of Ag was determined using thermogravimetric analysis in the range of 25–700 °C (Etemadzade et al., 2016).

4.2. Chemical method

Huy and co-researchers applied the electrochemical method to synthesise AgNPs with trisodium citrate as a reagent and stabilizer. The first sign of the nanoparticle formation was a colour change from transparent to yellow. An absorption peak of 406 nm was recorded using a UV–Visible spectrophotometer. The AgNPs were mostly spherical and homogenous and had a size range between 4 and 9 nm. The EDX confirmed the presence of elemental silver between 2.5 and 4 keV (Huy et al., 2017). Chitosan was used as a stabilizer in the synthesis of AgNP using the chemical reduction method. A colour change to yellow was noticed on the addition of sodium borohydride ($NaBH_4$), while UV–Vis with a λ_{max} 401 nm supported the formation of AgNPs. The TEM indicated spherical NPs with an average diameter of ≈14 nm. The EDX showed highly crystalline particles with a d-spacing of 0.23 attributed to the metallic silver (Dung et al., 2019). Using radiochemical synthesis, some AgNPs were designed to be immobilized on textile fabrics by Seino et al. The fabric turned yellow on the formation of AgNPs, with ICP measurement putting the amount of AgNPs on the textile fabric at 146 μg-Ag/g-fibre. TEM micrograph showed Ag particles in the range of 2–10 nm (Seino et al., 2016).

Graphene oxide (GO) powders were dispersed in a solution of $AgNO_3$ and ethylene glycol, followed by mixing and pulse microwave-assisted synthesis to form a solution of AgNPs of graphene oxide. The NP solution formed was dried in vacuo. High-resolution transmission electron microscopy (HR-TEM) and field emission scanning electron microscopy (FE-SEM) was used to characterize the morphology of graphene oxide, the graphene oxide mediated AgNPs and the distribution of Ag particles on graphene oxide sheets. Other characterization techniques employed include XRD, X-ray photoelectron spectrometer, atomic force microscope and thermogravimetric analyzer. The HR-TEM image revealed a thin transparent black layer of GO sheets and folded edges with small wrinkles. Spherical particles were observed by the FE-SEM, indicating the successful attachment of Ag particles evenly on the GO sheets. The size distribution of the particles was between 5 and 25 nm, with an estimated 10% Ag load per gram of GO sheets and a thickness distribution of 0.6–9.0 nm (Chen et al., 2016). Similarly, adsorption of AgNPs on the surface of graphene oxide sheets was applied to prepare some graphene-based Ag composites. The AgNPs were uniformly adsorbed onto the surface of GO with sizes distributed between 30 and 50 nm in form of well-dispersed aqueous colloidal hybrids (Elazzazy et al., 2017). Joe and co-workers applied a spark discharge generation (SDG) system to prepare AgNPs coated air filter with a geometric standard deviation and mode diameter of approximately 1.5 and 11 nm respectively. The coating efficiency of the filter sample for $AgNO_3$ was reported to be ≈41.7% in mass base and ≈89.6% in number base (Joe et al., 2016).

4.3. Biological method

Avilala & Golla used $AgNO_3$ and actinomycetes isolated from mangrove soil in the biosynthesis of AgNPs of *Nocardiopsis alba* extract. The formation of the NPs was confirmed with a colour change from colourless to brown. UV–Vis absorption peak of 420 nm indicated the presence of AgNPs coupled with FTIR band at 564 cm^{-1} which was assigned to AgNP vibration. The XRD and TEM also indicated the formation of spherical crystalline AgNPs of 20–60 nm with an average size of 32.5 nm (Avilala and Golla, 2019). AgNPs of collagen was also prepared by mixing 40% 1 mM of AgNPs with 40% (v/v) collagen, 10% (v/v) PBS, 6.4% of 0.2 M NaOH and 3.6% H_2O on ice. The AgNPs were confirmed using electron microscopy and much focus was on their interesting biological applications (Zhang et al., 2017). Some AgNPs were biosynthesized from pure honey and $AgNO_3$. The result of the UV–Vis spectrophotometer depicted an absorption peak at around 340 nm. Results from TEM showed spherical NPs with sizes ranging from 20 to 50 nm in diameter (Zeedan et al., 2020).

Similar to the AuNPs reported by El-Sheek and co-researchers, *Oscillatoria* sp. and *Spirulina platensis* was used in the biosynthesis of respective AgNPs upon reaction with $AgNO_3$. The microalgae were reported to have the ability to reduce the metallic ions intracellularly or produce nanoparticles extracellularly. The cells were broken up by subjecting them to mechanical mashing at room temperature for an hour to ensure the release of the NPs, which were then washed at 50 °C. The synthesized NPs were characterized using UV–Vis, FTIR, TEM and XRD. The AgNPs formed were revealed as spherical structures of sizes 14.42–48.97 nm with confirmed capping, reducing and stabilising effects of the algae polysaccharides and proteins (El-Sheekh et al., 2020). Flupep, a peptide inhibitor of the influenza virus was used to functionalize AgNPs by adding the ligand mixture to the NPs before getting vortex-mixed. It was explored as a delivery system for Flupep and increased its antiviral activity (Alghrair et al., 2019).

Choudhary et al. recently demonstrated the impregnation of *Citrus limetta* peels that had been washed, dried and milled to powder form by $AgNO_3$. The impregnated biomass was filtered, washed and dried and characterized using XRD and XPS which confirmed metallic forms of silver. The characterization results showed a change in surface morphology of the biomass from smooth to rough and heterogeneous. This indicates the successful impregnation of Ag which was later found as 7.25 wt% content (Fig. 2). The AgNPs size was averagely reported as 5 nm (Choudhary et al., 2020). In another study, silver nitrate was added to microbial filtrates of some mosquitocidal *Bacilli* and then incubated at room temperature. The formation of AgNPs was indicated by the appearance of a brownish solution. FTIR confirmed the presence of protein biomolecules through free amide groups on the spectra. The size of the NPs ranges from 15 to 21 nm from dynamic light scattering (DLS) readings, and further examination was conducted using UV–vis, TEM, SEM and energy-dispersive x-ray spectroscopy (EDX) (El-Bendary et al., 2019).

Silver NPs were biologically synthesized using $AgNO_3$ and bacterial filtrate of *Bacillus subtilis* as a reducing agent. A visual change in colour from pale yellow to brown in the solution was noticed, suggesting the formation of AgNPs. UV–Vis was used to follow the formation of the AgNPs where the SPR of the synthesized AgNPs was found between 420 and 430 nm. The presence of Ag was further confirmed by optical absorption peak at 3 KeV, using EDX spectroscopy. ZP measurement showed the nanoparticles to be negatively charged with a value of −40 mV. HRTEM was used to detect the crystallinity, shape and size of the NPs, with the results showing the particles to be irregular, hexagonal and spherical. Polydispersity index of 0.331 and average dynamic size of 20 nm were recorded using DLS. The FTIR spectrum indicated that the AgNPs were capped with reducing biomolecules (El-Bendary et al., 2020). Similarly, three series of AgNPs were biosynthesized using $AgNO_3$

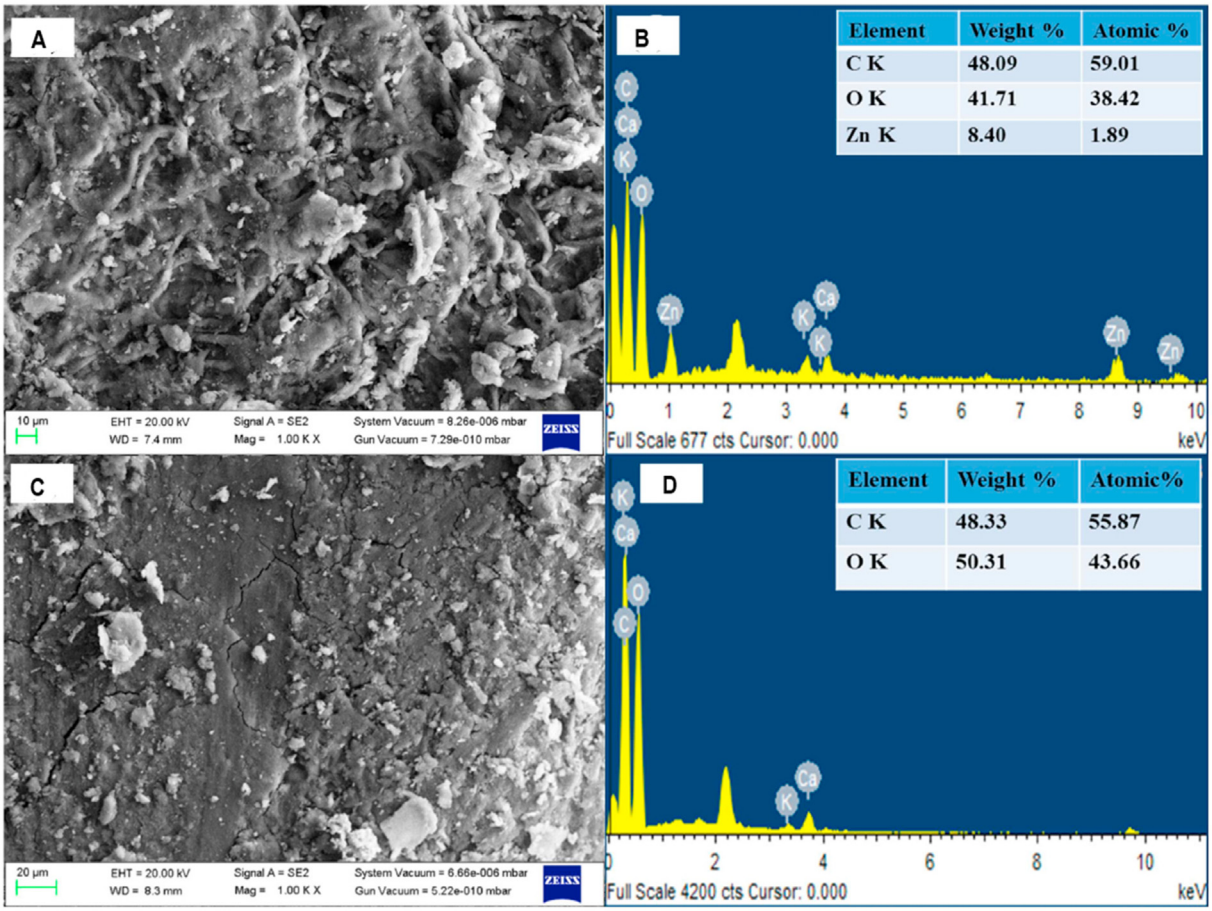

Fig. 2. SEM-EDX analysis of zinc impregnated and raw *Citrus limetta* peels: Fine powdered sample followed by gold coating produced high-resolution images for surface morphology and elemental composition data (A) FE-SEM images for zinc impregnated *Citrus limetta* peels represented rough surface morphology, clearly depicting that ZnO NPs have embedded inside the biomaterial (B) EDX analysis result of zinc impregnated *Citrus limetta* peel shows a peak for zinc justifying the presence of ZnO NPs (C) FE-SEM images for raw *Citrus limetta* peels represented a smooth morphology and its EDX graph (D) contains no peak for zinc. (Reproduced with permission from (Choudhary et al., 2020), Copyright (2020) Elsevier B. V.).

and *Bacillus* sp. The progression of the synthesis was monitored using UV–Vis spectroscopy with a colour change from pale yellow to brown, indicating the formation of the NPs. EDX confirmed the presence of elemental Ag in the NPs at 20 keV. The DLS recorded for the three NPs were 80, 92 and 77 nm, while the ZP were −18.5, −16.6 and −21.3 mV respectively. The TEM images showed triangular, hexagonal and spherical NP shapes (Elbeshehy et al., 2015).

Aqueous extract of *Cinnamon cassia* was used to reduce $AgNO_3$, leading to the synthesis of its AgNPs. The absorption of the NPs was measured on a UV–Vis spectrophotometer, showing a single broad peak at 410 nm. Using SEM, the average size of the NPs was recorded as 42 nm with spherical shapes. Slight variation in the FTIR bands for *Cinnamon* and AgNPs of *Cinnamon* at 688, 1634, 2,077, and 3,455 cm^{-1}, and 674, 1637 and 3433 cm^{-1} respectively were suggestively attributed to the formation of NPs (Fatima et al., 2015). The extract of *Neochloris aquatic* and $AgNO_3$ solution was used to synthesize green AgNPs which was primarily confirmed by a colour change from light yellow to brown. Further characterization was conducted using UV–Vis in the range of 200–700 nm and the SPR was recorded at 428 nm. The average size of the AgNPs was found to be approximately 20 nm using XRD analysis. The EDX showed an optical absorption peak of the NPs as 3.0 keV, and a spherical shape for the AgNPs was observed by the HRTEM micrograph (Tamil Selvan et al., 2019).

Moringa oleifera extract was used by Sujitha and co-workers to reduce $AgNO_3$ in the biosynthesis of a dark brown AgNP solution. The AgNPs were characterized using UV–Vis with λ_{max} at 450 nm. The NPs were spherical with an average size of 100 nm. The EDX showed a strong optical absorption band peak attributed to metallic Ag at 3.0 keV. Intense peaks corresponding to (111), (200), (220) and (311) Bragg's reflection based on the face-centred cubic structure of the AgNPs was read on the XRD pattern. Readings from the FTIR spectrum suggested that molecules capping AgNPs may have both free and bound amide groups (Sujitha et al., 2015). Ginseng (*Panax ginseng*) root extract was used as a reducing agent on $AgNO_3$ before being subjected to ultra-sonification for nearly 3 h. A yellow solution was formed indicating the formation of AgNPs. The absorption peaks of the AgNPs were found at 465 nm using a UV–Vis spectrophotometer. The green-synthesized NPs have a cubic crystal system and a size ranging between 9 and 11 nm, with TEM analysis showing spherical shape and size between 5 and 15 nm. EDX was used to confirm the presence of elemental Ag and the crystalline nature of the NPs was confirmed by XRD (Sreekanth et al., 2018).

Granular activated carbon (GAC) was prepared from oil palm shells and impregnated by Ag at different concentrations using the incipient wetness impregnation method. The particle size of the NPs was reported between 25 and 40 nm. TEM micrographs of the Ag-impregnated GAC showed an average diameter of <50 nm and ZP between −30 and −40 mV. The GAC and impregnated GAC were characterized using XRD with the observed peaks similar to diffraction patterns of silver in Ag^0 form (Shimabuku et al., 2017). Green synthesis method was also applied to synthesize three different AgNPs of plant extracts (*Andrographis paniculata, Phyllanthus niruri* and *Tinospora cordifolia*). A colour change from light yellow to yellowish-brown was attributed to the reduction of Ag

ions into AgNPs. The absorption maxima in the range of 420–455 nm were recorded for the three AgNPs. Using SEM, the average size of the three NPs falls between 50 and 120 nm. Identification of functional groups in the extracts was done using FTIR. Further characterization was done using DLS and ZP measurement. The NPs were observed to be polydispersed with a particle size less than 100 nm and ZP of −21.4 mV, −20 mV and −17.0 mV for *A. paniculata, P. niruri,* and *T. cordifolia* respectively (Sharma et al., 2019). Extract of *Bruguiera cylindrical* and $AgNO_3$ was used in the synthesis of AgNPs, which was confirmed by UV–Vis absorption peak at 430 nm. The shape of the NPs was mostly spherical, with an average size of 30–70 nm according to the results of SEM analysis. FTIR showed the presence of the following functional groups; amine, carboxylic acid, alkene and alkane. The EDX confirmed the presence of elemental silver around 3.0 keV and XRD pattern showing its crystallinity (Murugan et al., 2015).

Extracts of green tea and coffee were added individually by Rónavári et al. to $AgNO_3$ solution to form AgNPs. The two AgNPs underwent characterization to determine their properties. Peak maxima of AgNPs of the green tea and coffee were found at 456 nm and 469 nm characteristics to SPR respectively. Both showed spherical morphology from the TEM analysis. The mean size of AgNPs of green tea and coffee were 12.7 nm and 3.2 nm respectively while the XRD pattern of the two NPs displayed four intense characteristics reflections at 2-theta angles of 38.2°, 44.3°, 64.4°, and 77.4°, corresponding to (111), (200), (220), and (311) planes of the face-centred cubic lattice structure of metallic Ag (Rónavári et al., 2017). Curcumin acted as both a capping and reducing agent when reacted with $AgNO_3$ for the synthesis of AgNPs. The absorption maxima of the NPs were read at 406 nm using the UV–Vis while DLS indicated a 45 nm size with a ZP of −24.6 mV (Sharma et al., 2017). Haggag et al. synthesized reddish-brown AgNPs by adding hexane fraction of *Lampranthus coccineus and Malephora lutea* to $AgNO_3$. The result of TEM analysis showed that the NPs are spherical, with average sizes between 0.12 – 27.89 nm and 8.91–14.48 nm respectively. The maximum absorbance of the NPs was found at 417 nm. FTIR was employed to detect the functional groups present (Haggag et al., 2019). Kaushik et al. also reported a green synthesis of AgNPs using *Carica papaya* extract with a colour change from light yellow to yellowish-brown. A broad SPR was observed within the range of 400–440 nm. SEM images of the NPs indicated that the NPs are spherical with size in the range of 64–151 nm (Kaushik et al., 2019). $AgNO_3$ was added to the total extract and petroleum ether fraction of *Amphimedon* sp. resulting in reddish-brown AgNPs. The result of TEM analysis indicated the NPs to be spherical with particulate sizes of 8.22–14.30 nm and 8.22–9.97 nm for the total extract and petroleum ether fraction of *Amphimedon* sp. respectively. The absorbance recorded using UV–Vis were 450 and 415 nm respectively while FTIR indicated the presence of phytochemicals in the NPs (Shady et al., 2020).

In another study, amantadine, an antiparkinson drug was used to synthesize AgNPs by mixing Vitamin C, $AgNO_3$ and Amantadine. The NPs were sonicated before passing through the filter. Using TEM to characterize, the NPs showed uniform and monodisperse spherical morphology, with AgNPs and AgNPs of amantadine having 3 and 2 nm average particle size respectively. The ZP of Ag-amantadine was found to be −29 mV, which was lower compared to −14 mV recorded for AgNPs (Li et al., 2016a). Similar research was conducted in the same year by the author using oseltamivir instead of amantadine and vitamin C to reduce $AgNO_3$ followed by the addition of oseltamivir, similarly to the earlier procedure. The NPs were characterized by TEM, showing uniform, monodispersed spherical particles with an average size between 2 and 3 nm. ZP of −16 mV was recorded for AgNPs which was higher than −27 mV recorded for Ag-Oseltamivir (Li et al., 2016b).

In a green synthesis involving protein biomolecules, $AgNO_3$ was reduced using vitamin C, with the resulting NPs added to PEI and (small interfering RNA) siRNA to form silver nanocomposites of PEI and siRNA. The PEI and siRNA were used to cap the AgNPs, with the formation of nanocomposites shown by a strong absorption band at 420 nm through UV–Vis spectroscopy. TEM images showed Ag-PEI- siRNA to be uniform and spherical. The ZP of AgNPs, Ag-PEI and Ag-PEI-siRNA were −18 mV, 40 mV and 17 mV respectively. The PDI value of 0.065 was recorded for Ag-PEI-siRNA and a positively charged ZP of +18 (Li et al., 2017). Commercially available poly-vinyl pyrrolidone coated AgNPs (PVP-AgNPs) of the size distribution of 8–12 nm, absorption peak of 390 nm, optimal density of 155 cm^{-1} and mass concentration of 1 mg/mL were reported as well of those with 10 nm at 20 ppm stock (Morris et al., 2019; Jeremiah et al., 2020). Ramadan et al. reacted an aqueous extract of *Melaleuca alternifolia* and $AgNO_3$ to produce reddish-brown AgNPs with turbidity standard determined as 600 nm. The green NPs were characterized using TEM, PDI and ZP. Results derived from TEM analysis showed the NPs to be spherical with a mean size of 11.56 nm. A negative value of ZP at −28 mV was recorded alongside a PDI of 0.172 (Ramadan et al., 2020). The summary of the synthetic method and physicochemical properties of the overviewed AuNPs is presented in Table 2.

5. Antiviral activities of gold and silver nanoparticles

Generally, Au and Ag NPs have been recently reported with interesting antiviral activities suggestively due to their multi-targeting mechanisms of action (Fatima et al., 2015). The expression of antiviral activities of the NPs varies across the broad classes and sub-classes of the viral genomes. The broad classes include the DNA viruses with genome replication initiated by either the virally encoded DNA polymerases or the host and the RNA viruses with genome replication by the virally encoded RNA-dependent RNA polymerase (RdRp). Whilst the former class consists of the single-stranded (genome <2 kb) and double-stranded (genome >375 kb) types, the latter is made up of the positive- and negative-stranded RNA subtypes (Payne, 2017a, 2017b). For easier analysis, the antiviral activities of the NPs were further addressed based on the systemic viral infections.

5.1. Influenza virus

Influenza virus, popularly referred to as flu, is responsible for contagious influenza in some mammals and birds and is characterized by a non-segmented negatively sensed RNA genome. Its main subtypes are A, B and C with subtype A being the most virulent, widespread and pinpointed in influenza outbreaks (Morris et al., 2019). An M2e peptide AuNP-based vaccine (AuNP-M2e-sCpG) formulated by Tao and co-researchers was evaluated in mice infected with different strains of the influenza A virus. The vaccinated mice posted 100%, 100% and 92% protection against lethal doses of A/California/04/2009 (H1N1pdm) pandemic strain, A/Vietnam/1203/2004 (H5N1) and A/Victoria/3/75 (H3N2) respectively. Through intranasal delivery, the NP in the presence of a soluble adjuvant, CpG (AuNP-M2e + sCpG) was demonstrated to significantly induce activation of lung B cell and serum anti-M2e immunoglobin G (IgG) response, and stimulation of 1 and 2a IgG subtypes (Fig. 3) (Tao et al., 2017). The result indicates the antiviral potentials of the NP worthy of translational study into a vaccine against influenza A. Gold and silver NPs of Flupep were also tested alongside the free Flupep ligand for activity against influenza. Both NPs of Flupep inhibited the viral plaque formation in canine MDCK cells, with free Flupep ligand showing lower activity, indicating that conjugation between the NPs and Flupep increased the antiviral activity (Alghrair et al., 2019).

Cinnamon bark extract and its AgNPs were evaluated at various concentrations for antiviral activity on Vero cells infected with influenza H7N3 subtype and tetrazolium dye MTT assay for viability. The cinnamon bark extract showed high efficacy against influenza virus in both assays when co-incubated with the virus pre- and post-infection, quantified by IC_{50} of 242 and 316 μg/mL respectively while higher inhibitory effects were observed with the AgNPs, indicated by IC_{50} of 101 and 125 μg/mL respectively. Although, the exact mechanisms of action could

Table 2
Physicochemical properties of silver nanoparticles with antiviral potentials.

Precursor material	Method of synthesis	Colour	λ_{max} (nm)	Size/shape of NPs	Zeta potential	Polydispersity index	References
Bacillus subtilis	Biological	Brown	420 to 430	20 nm/irregular, hexagonal, spherical	−40 mV	0.331	El-Bendary et al. (2020)
Nocardiopsis alba	Biological	Brown	420	32.5 nm/polydispersed, spherical	NA	NA	Avilala and Golla (2019)
Honey	Biological	Brown	340	20–50 nm/spherical	NA	NA	Zeedan et al. (2020)
Spirulina platensis and *Oscillatoria* sp.	Biological	Brown	432	14.42–48.97 nm/ spherical	NA	NA	El-Sheekh et al. (2020)
Citrus limetta	Biological	NA	NA	5 nm	NA	NA	Choudhary et al. (2020)
$NaBH_4$	Chemical	Yellow	401	14 nm/spherical	NA	NA	Dung et al. (2019)
Mosquitocidal *Bacilli*	Biological	Brown	386–412	10–33 nm/consistent, hexagonal, spherical, oval and cuboidal	−23.6 to −30.6 mV	0.313–1.000	El-Bendary et al. (2019)
Bacillus spp.	Biological	Brown	425	77–92 nm/triangular, hexagonal and spherical	−16.6 Mv to −21.3 mV	NA	Elbeshehy et al. (2015)
Cinnamomum cassia	Biological	Dark brown	410	42 nm/spherical	NA	NA	Fatima et al. (2015)
Neochloris aquatic	Biological	Brown	428	15–20 nm/spherical	NA	NA	Tamil Selvan et al. (2019)
Moringa oleifera	Biological	Dark brown	450	100 nm/spherical	NA	NA	Sujitha et al. (2015)
Panax ginseng	Biological	Dark yellow	456	5–15 nm/spherical	NA	NA	Sreekanth et al. (2018)
Andrographis paniculata, Phyllanthus niruri, Tinospora cordifolia	Biological	Yellowish brown	420–455	50–120 nm/spherical	−17 mV to −21.4 mV	NA	Sharma et al. (2019)
Bruguiera cylindrica	Biological	Yellowish brown	430	30–70 nm/spherical	NA	NA	Murugan et al. (2015)
Melaleuca alternifolia	Biological	Reddish brown	NA	11.56 nm/spherical	−28 mV	0.172	Ramadan et al. (2020)
Tannic acid and sodium citrate	Chemical	Brown	408	24 nm/spherical	−58 mV	NA	Orłowski et al. (2018)
Green tea and coffee	Biological	NA	456 469	12.7 nm 3.2 nm/spherical	NA	NA	Rónavári et al. (2017)
C. papaya	Biological	Yellowish brown	400–440	64–151 nm/spherical	NA	NA	Kaushik et al. (2019)
Lampranthuscoccineus and Malephoralutea	Biological	Reddish brown	417	10.12–27.89 nm 8.91–14.48 nm/spherical	NA	NA	Haggag et al. (2019)
Trisodium citrate	Chemical	Yellow	406	4–9 nm/spherical and homogenous	NA	NA	Huy et al. (2017)
Amphimedon spp.	Biological	Reddish-brown	415–450	8.22–14.30 nm/spherical	NA	NA	Shady et al. (2020)

NA: Not available/not reported.

not be succinctly observed, however, the binding of the NPs to the viral envelope glycoprotein has been suggestively implicated as the pathway of preventing the viral infusion into host cells. Interestingly, neither the cinnamon extract nor its AgNPs exhibited daunting cytotoxicity (Fatima et al., 2015). The results potentiate cinnamon bark extract and its AgNPs as effective anti-influenza agents for future study.

Sulforhodamine B (SRB) assay was used to investigate the antiviral activity of the AgNPs against the influenza A virus. Slight inhibitory activities (4.18–5.97%) were observed at lower concentrations (0.005–0.15 M), which became apparent with increased concentration, peaking at a 15.12% rate at 0.25 M of AgNPs. Although no specific mechanism could be experimentally deduced, none of the screened concentrations was reported to have cytotoxicity towards uninfected MDCK cells (Sreekanth et al., 2018). The antiviral effects of Ag NPs were evaluated in terms of immobilisation on textile fabrics. At all Eagle's minimal essential medium concentration, ordinary cotton fabrics had a slight decrease in viral infectivity titer of Influenza A virus and Feline calicivirus while silver modified fabrics had a higher decrease in infectivity titer value compared to control. The deactivation of the AgNP was suggestively induced by the inhibitory agent through surface passivation (Seino et al., 2016). Li and co-workers evaluated the antiviral activity of AgNPs of Amantadine and oseltamivir *in vitro* against negatively stained influenza A subtype H1N1 virus using MTT assay and MDCK cells. The virus control normally is spherical or elliptical, containing capsid and virus matrix. The viral morphology was destroyed and viral edges were lost after treating with AgNPs of Amantadine for 30 min, demonstrating a direct interaction between the nanoparticle and virus leading to inhibition of the virus. Cell viability was highest for the AgNPs of Amantadine at 90% compared to AgNPs and Amantadine individually, which was reported to be 39% when H1N1 influenza virus was introduced to MDCK cells. Similarly, infection of MDCK cells with H1N1 influenza virus posted cell viability of 39%; Oseltamivir, 59%; AgNPs, 65% and AgNPs of Oseltamivir, 90% cell viability (Li et al., 2016b). The experimental results pose AgNPs of amantadine and oseltamivir as promising anti-influenza virus agents in better terms than AgNP and the parent drugs individually. Antiviral efficiency of the AgNP synthesized by spark discharge system was investigated against aerosolised bacteriophage MS2 virus (influenza A H1N1) particles. The NPs were coated onto a medium air filter while densities and dust amounts were observed with differing coating areas after 15 min of exposure. The efficiency was reported to be on the increase with various coating area densities but decreased with dust amounts (Joe et al., 2016), indicating the propensity of the NPs to prevent viral survival on the surface.

5.2. *Respiratory syncytial virus*

Respiratory syncytial virus (RSV) is characterised by an aetiological viral infection of the respiratory system, commonly to children with no specific therapeutic option. Some AgNPs by Morris et al. were assessed *in vitro* at concentrations of 0, 10, 25 and 50 μg/mL by plaque assay for its effect on RSV infection using two epithelial A549 and Hep-2 cell lines. Significant dose-dependent inhibition of RSV replication and blockage of viral infusion into host cells was observed, indicated by the highest activity at 50 μg/mL. Suggestively as a novel *in vivo* experimental investigation of AgNPs on RSV-

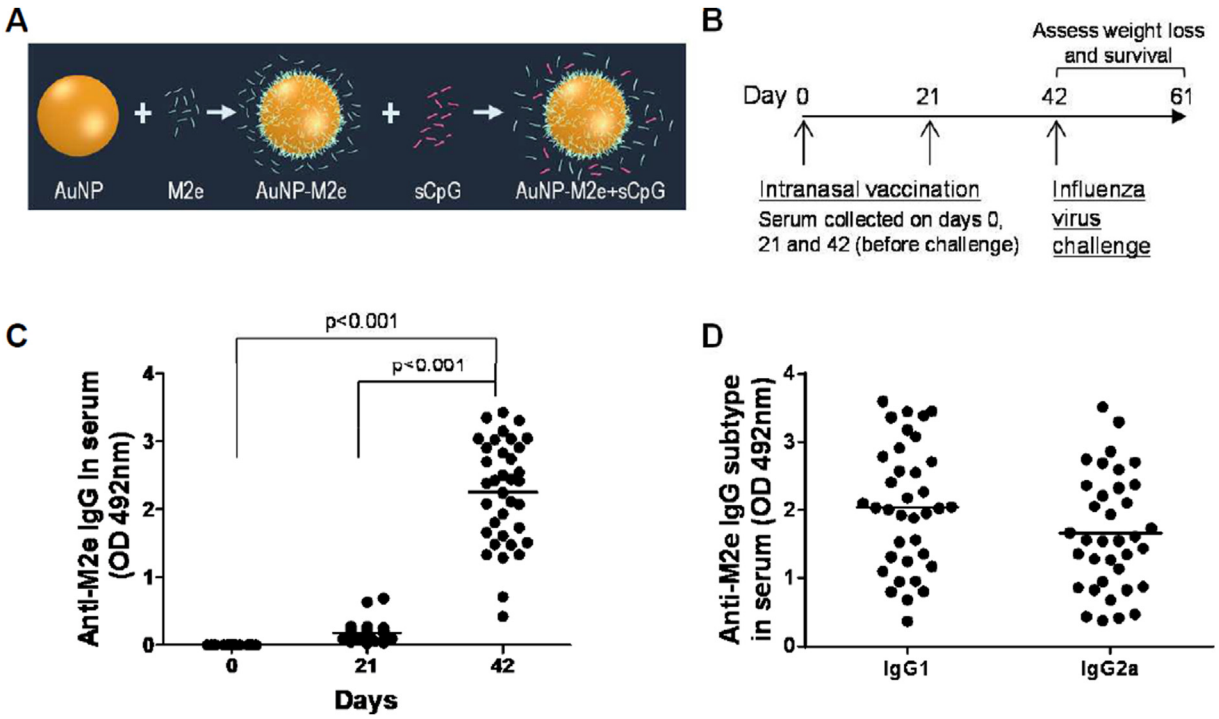

Fig. 3. (A) **Scheme of vaccine design.** M2e is conjugated to AuNPs. By keeping M2e in excess in the solution, complete surface coverage of AuNPs with M2e is ensured at all times. Soluble CpG (sCpG) is an unmethylated CG-rich oligonucleotide found in viral and bacterial genomes. sCpG is a known TLR-9 agonist, which enhances the immune response and is used as an adjuvant in the formulation. We used CpG 1826: 5′-TCCATGACGTTCCTGACGTT-3′ with phosphorothioate linkages. sCpG stays in solution and does not attach to AuNPs. (B) **Vaccination schedule**. Mice (n = 37) were vaccinated with AuNP-M2e+sCpG on days 0 and 21, and serum was collected on days 0, 21 and 42 for analysis. (C) **M2e-specific IgG antibody response in mouse serum.** M2e-specific IgG antibody in 1:1600 diluted serum of individual mice at days 0, 21 and 42. Each circle* represents an individual animal and the horizontal bar represents the mean. (D) **M2e-specific IgG1 and IgG2a response in mouse serum.** M2especific IgG1 and IgG2a antibodies in 1:1600 diluted serum of individual mice at day 42. Each circle* represents an individual animal and the horizontal bar represents the mean. The optical density (OD) of the ELISA reaction was measured at 492 nm wavelength. *: Serum of one vaccinated mouse was not available in sufficient quantity and it was thus not included in the ELISAs (Reproduced from (Tao et al., 2017), Copyright (2017) Elsevier Inc.).

infected mice. The biomaterials induce a reduction in pro-inflammatory cytokines and chemokines, activation of lung tissue, increment in neutrophils, chemoattractant CXCL1, granulocyte colony-stimulating factor (G-CSF) and granulocyte-macrophage colony-stimulating factor (GM-CSF) studied using Bio-plex, ELISA, and qRT-PCR analyses (Fig. 4) (Morris et al., 2019). The interesting anti-RSV activity at various experiments and insignificant cytotoxicity after 24 h exposure at lowest and highest doses of 10 and 50 μg/mL respectively support the potentials of the AgNPs to prevent and treat RSV upon further investigations.

5.3. Adenoviruses

Two types of AuNP, type 'a' consisting of Au sphere of diameter 1.5–20 nm, shelled with SiO_2 of diameter 12–30 nm and type 'b' Au sphere of diameter 2–20 nm coated onto SiO_2 aggregate sphere diameter were screened for their cytotoxicity and activity against adenovirus at different concentrations using Mardin-Darby bovine kidney (MDBK) and Hep-2 cell line, representing larynx epidermoid carcinoma. Silica, the carrier particles exhibited zero activity. The two AuNPs-SiO_2 showed anti-adenoviral activity with varying degrees of inhibition of the virus reproduction, especially the type 'b' even at low concentrations (Table 3) (Lysenko et al., 2018).

5.4. Severe acute respiratory syndrome coronaviruses

Silver NPs of various sizes and concentrations were evaluated for antiviral efficacy against SARS-CoV-2 *in vitro* TMPRSS2-inclined Vero E6 and Calu-3 cells. The materials demonstrate strong antiviral potentials through the inhibition of viral replication and disruption of viral integrity to prevent viral entry at diameter and concentrations of 10 nm and 1–10 ppm respectively. The NPs also inhibit extracellular SARS-CoV-2 and display a systemic tolerability with cytotoxic effect occurring ≥20 ppm (Fig. 5) (Jeremiah et al., 2020). From theoretical molecular dynamic simulations, AuNPs functionalised by various chemical groups such as undecane sulfonic acid, octane thiol and 3-mercaptoethyl sulfonate display stronger and more stable ligand-receptor interactions with RNA-binding domain (RBD) of SARS-CoV-2 than angiotensin-converting enzyme 2 (ACE2). The theoretical data supports the propensity of the functionalised AuNPs to compete with ACE2, in receiving the viral infusion, thereby inhibiting the viral entry (Mehranfar and Izadyar, 2020).

The mediation of heptad repeat 1-heptad repeat 2 (HR1-HR2) complex of the virus-host cells membrane fusion has been implicated as a major pathway of MERS-CoV infection, as such constitutes a potential therapeutic target. A peptide pregnancy-induced hypertension (PIH) reportedly demonstrates a strong inhibitory potential against the complex formation, quantified as IC_{50} of 1.171 μM, the activity of which became enhanced in 10-folds upon modification into gold nanorods (PIH-AuNRs). The particles interestingly display good biocompatibility and metabolic stability *in vitro* and *in vivo* thus representing a promising therapeutic model against MERS-CoV infection for further study (Fig. 6) (Huang et al., 2019). In another report, AuNPs as an adjuvant and a carrier induces a strong antigen-specific IgG response *in vivo* mice experimental model against SARS-CoV infection (Sekimukai et al., 2020).

5.5. Rotavirus

Rhesus rotavirus (RRV) strain MMU 18006 was introduced in MA104 cells with plaque assay method to quantify anti-RRV effects of

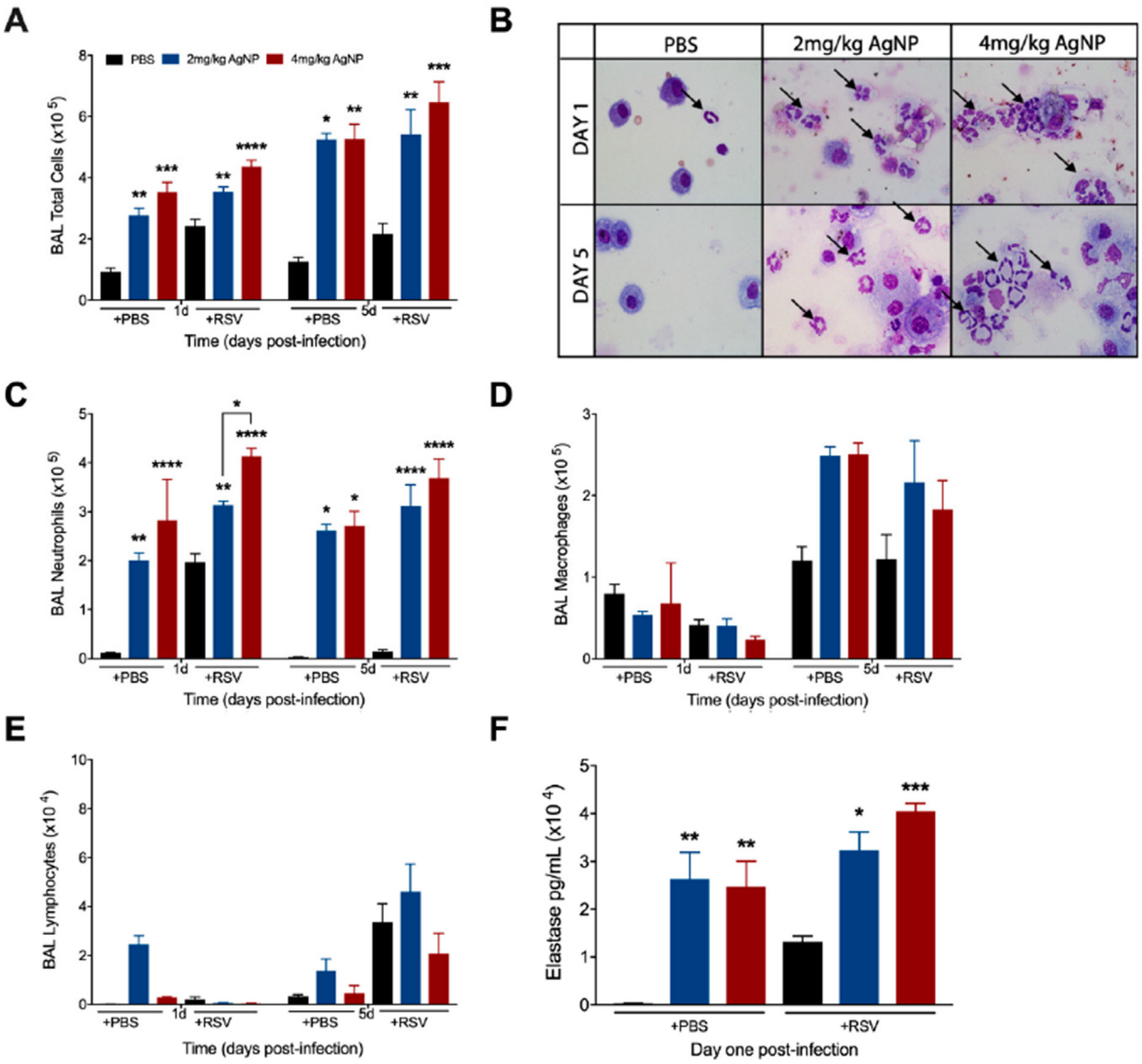

Fig. 4. AgNPs increase recruitment and activation of neutrophils to the lung, regardless of infection status. Mice were inoculated with PBS, AgNP-PBS (2 mg/kg or 4 mg/kg), RSV (5×10^6 PFU) or AgNP-RSV. At days one and five p.i., BALF was collected from all groups and used to obtain (A) total cell counts, as well as differential cell counts consisting of (C) neutrophils, (D) macrophages, and (E) lymphocytes. (B) BALF samples collected at days one and five p.i. from PBS untreated and AgNP-PBS mice were spun on glass slides, stained with H&E, and observed under a light microscope at 40× magnification. The black arrows indicate neutrophils. (F) Neutrophil elastase concentrations were measured by ELISA using BALF collected at day one p.i. Data are expressed as mean ± SEM ($n \geq 6$ mice) and is representative of three independent experiments. Significant results as compared to the respective control are marked with asterisks, and additional comparisons between groups are indicated with brackets (* for $p \leq 0.05$, ** for $p \leq 0.01$, *** for $p \leq 0.001$, **** for $p \leq 0.0001$) (Reproduced from (Morris et al., 2019), Licensed under CC BY 4.0).

some AgNPs. Using mice infected with biliary atresia, a viral infection associated with the neonatal system, a close to a total reduction of biliary epithelial cells at 9 and 12 days of RRV inoculation and a significant increase in survival in mice, reduction in jaundice and weight loss was recorded for the NP-treated group (Fig. 7). The proposed mechanisms include reduction in viral loads and upregulation of the transcripts for TGF-β mRNA in mice. The systemic tolerability of the NPs has indicated the bilirubin metabolism and liver enzymes which remain normal upon treatment, although, the AgNPs was found to be cytotoxic at high concentrations. Further analyses by flow cytometry and immunohistochemical staining show the reduction in NK cells. The results from antiviral activity showed AgNPs can greatly increase the rate of survival of biliary atresia in rotavirus inoculated mice (Zhang et al., 2017).

The colourimetric method was used to test for the cytotoxic effect of the synthesized AgNPs, adding different concentrations of the NPs to cell lines. The antiviral activity of the NPs was tested against simian SA 11 rotaviruses (RV SA 11) using MTT analysis. The CC_{50} value of the AgNPs of mosquitocidal bacilli was recorded as ranging between 346 and 747 μg/mL. All the AgNPs subjected to testing exhibited strong antiviral activities against rotaviruses, showing reduction titer ranging from 0.5 to 2.75 $\log_{10}$ $TCID_{50}$ (El-Bendary et al., 2019). El-Bendary and co-researchers did further work on AgNPs of *Bacillus subtilis*, examining the cytotoxicity of the NPs to lung (A549), liver carcinoma human cell lines (HepG-2) and African green monkey kidney epithelial cell line (MA104) where their activities were shown against the cell lines as CC_{50} values of 212.5, 6.4 and 78.9 mg/mL respectively. High activity against rotaviruses was recorded for the AgNPs, indicating high protection of the MA104 cell line from the deleterious effect of rotavirus by incubating the virus with AgNPs before cell infection. This reduced the virus titer by 3.25 $\log_{10}$ $TCID_{50}$ (El-Bendary et al., 2020) and potentiate the NPs for further antiviral study.

Table3
Anti-adenoviral activity of the AuNP–SiO_2 nanocomposites in MDBK cell cultures.

Dilution of nanoparticles	Antiadenoviral activity			
	Nanoparticles of 'a' type		Nanoparticles of 'b' type	
	Optical density	% inhibition of adenovirus reproduction	Optical density	% inhibition of adenovirus reproduction
10^{-2}	1.4064 ± 0.027	85	1.59 ± 0.012	100
10^{-3}	1.4587 ± 0.101	96	1.583 ± 0.016	100
10^{-4}	1.33 ± 0.136	82	1.600 ± 0.018	100
10^{-5}	1.02 ± 0.053	65	1.49 ± 0.076	95
10^{-6}	0.85 ± 0.052	55	1.41 ± 0.071	90
Cell control	**1.610 ± 0.017**			
Virus control	**0.37 ± 0.02**			

(Reproduced from (Lysenko et al., 2018), Licensed under CC BY 3.0).

5.6. Norovirus

The antiviral effects of AgNPs labelled Ag30–SiO_2 particles were evaluated against bacteriophage MS2 and murine norovirus (MNV) in four different types of water at 5 °C and 20 °C respectively. Higher inhibition at more than 3 log_{10} reductions of bacteriophage MS2 was recorded for the particles in distilled water and tap water at 5 °C while no significant reduction was observed on surface or groundwater. At 20 °C, > 4 log_{10} reductions of MS2 was recorded after 24 h of exposure for the four water types. Antiviral activities of the silver NPs were also reported to be excellent against MNV. The AgNPs exhibited high activity against MNV in the four different types of water under consideration (Park et al., 2018). Cumulatively with another experimental investigation where filtration efficiency of AgNPs coated glass filter was recorded as 99.99% against MS2, T1 and T4 viruses (Park et al., 2020). This indicates the potentials of the AgNPs as effective disinfectants for treating viral-bound water, amenable for water treatment upon further evaluation.

5.7. Measles

Measles is an exanthematous viral disease with therapeutic challenges. Chloroauric acid ($HAuCl_43H_2O$) and Sodium citrate dehydrate

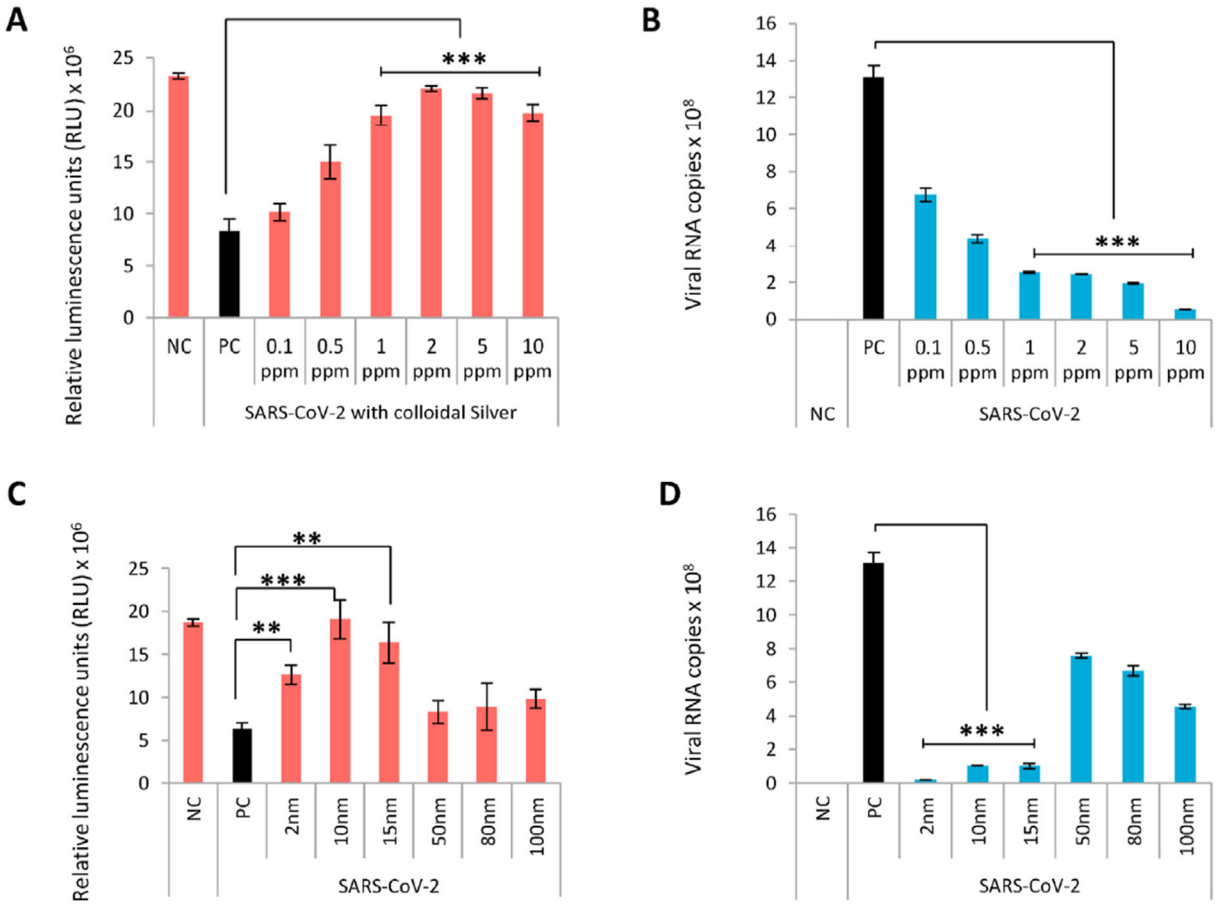

Fig. 5. Concentration- and dose-dependent antiviral effect of naked AgNPs on SARS-CoV-2. (A) Colloidal silver rescues Vero E6/TMPRSS2 cells from SARS-CoV-2 mediated cell death in a concentration-dependent manner. Error bars obtained from triplicate testing, *p*-value ≤0,005 (***). (B) Concentration-dependent inhibition of SARS-CoV-2 replication in Calu-3 cells by colloidal silver. Error bars obtained from triplicate testing, *p*-value ≤0,001 (***). (C) AgNPs exhibit size-dependent antiviral action against SARS-CoV-2 in Vero E6/TMPRSS2 cells. Error bars obtained from triplicate testing, *p*-value ≤0,005 (***). (D) Size-dependent viral inhibition of SARS-CoV-2 by AgNPs in Calu-3 cells. Error bars obtained from triplicate testing, *p*-value ≤0,001 (***). (Reproduced with permission from (Jeremiah et al., 2020), Copyright 2020, Elsevier Inc.).

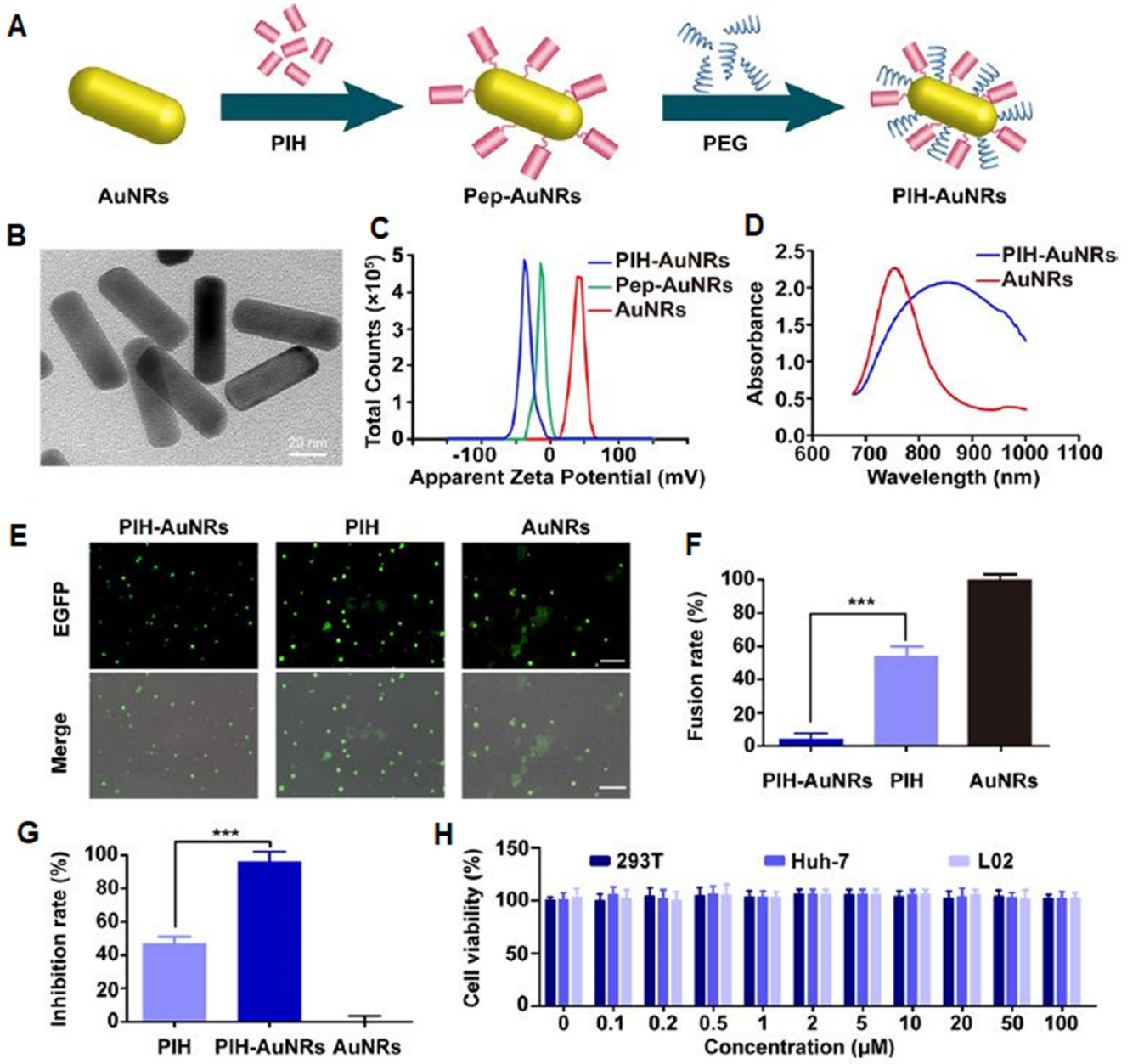

Fig. 6. Preparation, characterization and anti-MERS-CoV activity of PIH-AuNRs. (A) Preparation of PIH-AuNRs. (B) TEM images of PIH-AuNRs. Scale bar, 20 nm. (C) ZP of AuNRs, Pep-AuNRs and PIH-AuNRs. (D) UV–Vis spectra of PIH-AuNRs and AuNRs. (E) Representative images of cell fusion in the presence of PIH, AuNRs and PIH-AuNRs. Scale bar, 100 μm. (F) Quantification of cell fusion between Huh-7 and 293T/MERS/EGFP cells in the presence of PIH, AuNRs and PIH-AuNRs. (G) Inhibitory activity of PIH-AuNRs on MERS-CoV S2 subunit-mediated cell fusion. ***$p < 0.001$. (H) The cytotoxicity of PIH-AuNRs against 293T, Huh-7 and L02 cells for 48 h. The data are presented as mean ± sd (n = 10) (Reproduced with permission from (Huang et al., 2019), Copyright 2019, American Chemical Society).

(HOC(COONa) $(CH_2COONa)_2 2H_2O$) were used to synthesize colloidal AuNPs of Ribavirin by dissolving Ribavirin powder ($C_8H_{12}N_4O_5$) in AuNP. The suspension was kept in a dark bottle and shaken for 24 h at 37 °C. The AuNP-Ribavirin was separated from the excess ribavirin with the aid of centrifugation and washed with phosphate buffer saline. The antiviral activity of the synthesized AuNP analogue was evaluated against the measles virus (MV). The NPs showed higher efficacy notably at the post-infection stage compared to the parent drug. The result of the activities determined on Vero cells indicates a viral reduction of 78.1% on application of 99.5 μg/mL AuNPs of ribavirin and 25.4% reduction with 500 μg/mL ribavirin for the same viral concentration. The proposed mechanisms of antiviral action were traceable to ribavirin as the inhibition of the virus-coded RNA polymerase, thereby preventing the initiation and elongation of the viral mRNA and subsequently the infection and replication. The use of AuNP was concluded to increase the activity of ribavirin and reduce the dosage required, with the changes attributed to an increase in surface area and surface area to volume ratio (Ahmed et al., 2018). Meléndez-Villanueva et al. tested the antiviral activity of AuNPs of *A. sativum* (AuNPs-As) alongside the precursors ($HAuCl_4$ and garlic extract) against MV utilizing plaque formation units (PFU) assay, surface plasmon absorption and Vero cells viability, determined by MTT assay. At 10 μg/mL the antiviral activities of AuNPs of *A. sativum Allium sativum* (garlic extract) and chloroauric acid were 57.07%, 6.96% and 46.43% respectively, indicating higher efficacy of AuNPs-As against MV than the precursors. The AuNPs-As also demonstrated a strong inhibitory potential for viral replication in Vero cells quantitatively with EC_{50} and SI values of 8.829 μg/mL and 16.05 while $HAuCl_4$ shows 31.4 μg/mL and 7.4 respectively. The suggested virucidal mechanisms involve direct

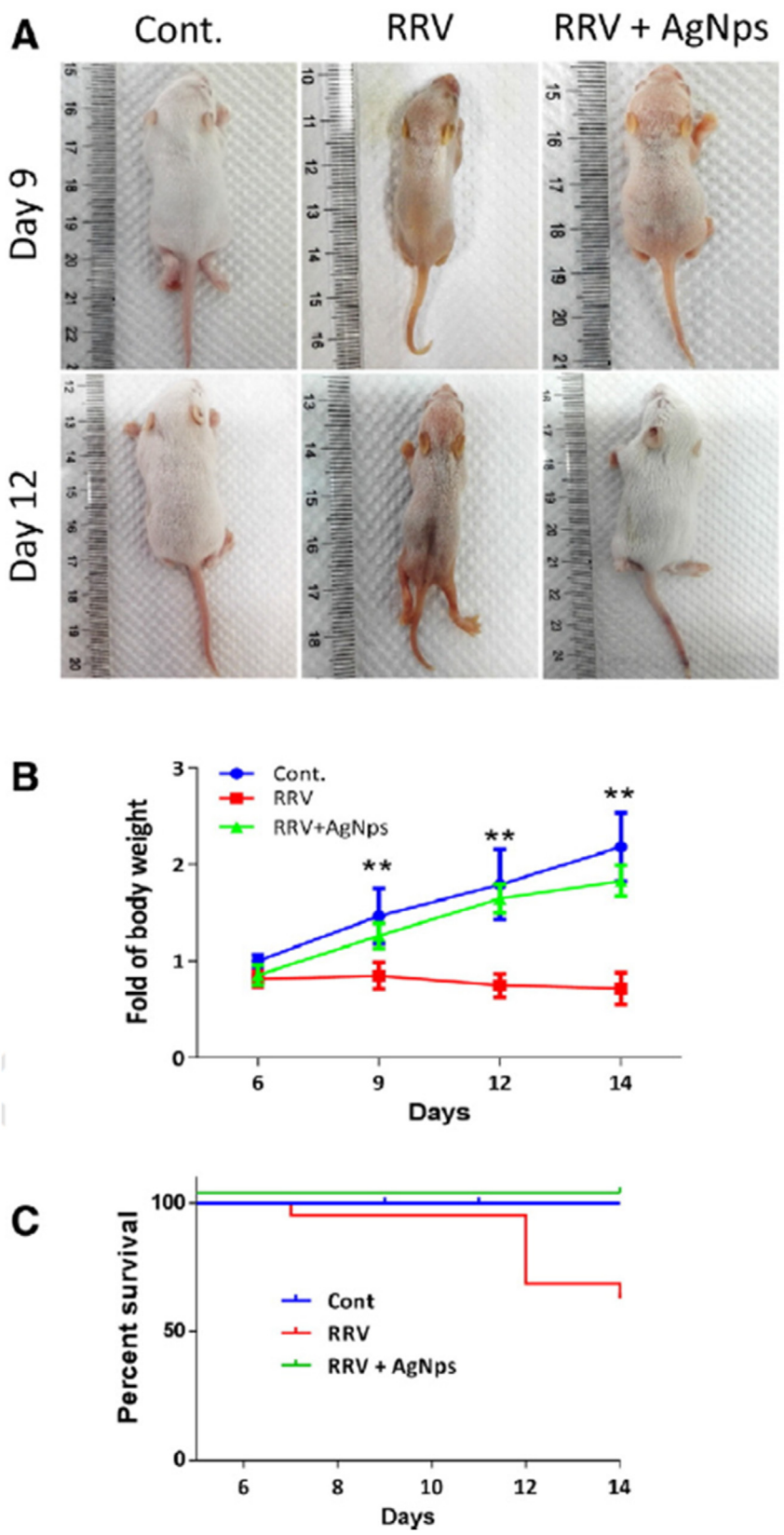

Fig. 7. Effect of AgNps on biliary atresia (BA) syndrome in rhesus rotavirus-induced BA mouse model. (A) The physical appearance of mice at days 9 and 12 after virus inoculation (RRV) alone and at days 3 and 6 after injection with AgNps (RRV + AgNps). (B) Weight of each group at different time points after injection with AgNps was recorded; the y-axis indicates the fold increase of weight, which was calculated relative to the weight of the control group at day 6. **P b 0.01, n = 16, 18 and 17 in Cont, RRV and RRV + AgNps group. (C) The survival curve of each group at different time points was recorded (Reproduced with permission from (Zhang et al., 2017) Copyright 2016, Elsevier Inc.).

blockage of viral particles (Meléndez-Villanueva et al., 2019). Although the mechanisms of action are not fully defined, the NPs display a promising strategy for controlling infections associated with MV and other enveloped viruses.

5.8. *Chikungunya*

Silver NPs of *Citrus limetta* peels were prepared along with Fe and Zn counterparts and evaluated for antiviral activity against Chikungunya

virus (CHIKV) using *in vitro* MTT assay in culture cells. The results showed that the particles possess strong antiviral activity, indicated by a significant reduction in viral titer of CHIKV and viral RNA level. Plaque reduction assays carried out in CHIKV-infected Vero cells show the antiviral activity of the NPs at 0.05 mg/mL, 0.1 mg/mL and 0.2 mg/mL, posting a greater than 90% inhibition at the tested concentrations. In the qRT-PCR analysis, a reduction in viral mRNA genomic expression was observed for all tested concentrations, 0.05, 0.10 and 0.20 mg/mL in inverse linearity. Using nonlinear regression curve fit method by graph pad prism software, IC_{50} and SI values of 11.73 μg/mL and 145.7 were recorded for the AgNPs, representing the most potent compared to Fe and ZnO counterparts with higher IC_{50} values of 15.52 and 40.67 mg/mL as well lower SI values of 109.5 and 33.5 respectively (Choudhary et al., 2020). The experiments need to be expanded for a better understanding of the mechanisms of activity, however, AgNPs of *citrus limetta* peels possess impressive antiviral potentials against CHIKV and other similar arthropod-borne alphaviruses for further nanomedicine development.

Cytotoxicity assays using Vero cells were used to evaluate the antiviral activity of AgNPs of *A. paniculata, P. niruri* and *T. cordifolia*. Among others, AgNPs of *A. paniculata* demonstrates the most cytotoxic effect with a maximum non-toxic dose (MNTD) of 31.25 μg/mL, compared to those of *P. niruri* and *T. cordifolia* with MNTD of 125 μg/mL and250 μg/mL respectively. The *in vitro* MTT assay displays AgNPs of *A. paniculata* with the highest CPE, indicated by cell viability which increased significantly from 25.69% to 66.86 and 80.76% on treatment of the CHIKV-infected cells with the NPs at ½ MNTD and MNTD respectively (Sharma et al., 2019). Although, a more experimental investigation is required especially *in vivo* for a better understanding of their mechanisms of action, however, AgNPs of *A. paniculata* could provide economic, safe and effective therapeutic options against CHIKV whose treatment options remain challenging. The antiviral effect of green AgNPs of *C. papaya* leaves was evaluated against CHIKV. The activity was measured in terms of CPE and increase of percentage viability. Using MTT assay, the inhibition of CHIKV have been observed as 39% and 52% inhibition when treated with 62.5 and 125 μg/mL, representing ½ MNTD and MNTD respectively of the NPs. The interesting results were supported by the cell viability which increased by 14% upon application of ½ MNTD of the NPs (Kaushik et al., 2019). The results further buttress the promising potentials of the green AgNPs for effective treatment of CHIKV which demand further scientific attention.

5.9. Human immunodeficiency virus

The human immunodeficiency virus (HIV) continues to pose threat to global wellbeing while the search for an effective therapeutic strategy lasts. The few available medications including the highly active antiretroviral therapy (HAART) are complicated with hypersensitivity, unpleasant aftereffects and contraindications, toxicity and incessant resistance, and the challenges of high viral mutation (Singh et al., 2019; Eggleton and Nagalli, 2020). Immune cells are renowned targets for the viral-host infusion, thereby forming a therapeutic target (Zazo et al., 2017). Other implicated therapeutic targets for HIV include the viral integrase enzyme for replication (Singh et al., 2019). Lately, some negatively charged Au-based glyconanoparticles reportedly displayed interesting potentials for modulating and stabilising the secondary structure of a gp120 V3 loop peptide implicated in the pathogenesis of HIV. They are therefore suggested for further study as HIV vaccine candidates (Gianvincenzo et al., 2015). Delivery of drug molecules to target host cells, resistance and toxicity contributively limit the efficacious applicability of most antiretroviral medications for treating HIV/AIDS infections. The combination of AuNPs interchangeably with synthesised O-palmitoylmannan (OPM) and Efaverinz enhanced the delivery through mannosylated niosomes and protein-carbohydrate intermolecular interactions between the lectins and mannan on gp-120 of HIV host cells and receptor respectively to improve antiviral effects. Quantitatively, the IC_{50} of AuNPs was reportedly higher than that of nanoparticle-inclined Efaverinz at 185.3 and 94.6 μg/mL respectively. The results demonstrate an enhanced delivery of the drug molecules through mannosylated niosomes by 42.6% compared to non-liganded noisome. The *in vitro* cumulative release, permeation and mucosal retention of both Au-loaded Efaverinz (EGNz) and the mannosylated type (manEGNz) were also demonstrated (Malik et al., 2018), a potential for overcoming the challenges of delivery associated with antiretroviral agents. Single-stranded RNA molecules were reportedly delivered through PEGylated AuNP analogue linked covalently to thiol-modified oligoribonucleotide using a cleavable linker group, N-succinimidyl 3-(2-pyridyldithio) propionate. The coatings of the NPs with polyethyleneimine enhance cell entry and endosomal escape, resulting in the uptake of ≈45000 RNA strands per lymphocyte. An extracellular aggregation was observed for the NPs with an only occasional presence within the cytoplasmic vesicle (Fig. 8). The modified NPs demonstrate a nanotechnology-dependent delivery, although, no antiviral activity was recorded when subjected to MTT cytotoxicity assay and antiviral assay against HIV suggestively due to inadequate intracytoplasmic delivery of the RNA molecules (Parboosing et al., 2018). An improved delivery of stavudine, an antiretroviral medication was demonstrated through Au nanocarriers. The AuNPs of stavudine reportedly activated a typical proinflammatory signal implicated in antiviral effects of macrophages, show better antiviral activity than the NPs of Au or stavudine separately (Zazo et al., 2017). The nanotechnology-based innovation supported by an earlier hypothesis of the hosting of AuNPs by human macrophages represents a potential therapeutic approach for HIV, deserving further exploration.

The conjugates of AuNP/hexapeptide and AuNP/hexapeptide/Tat peptide (where Tat = transactivator of transcription) synthesized by Singh et al. were investigated for cellular entry potential and integrase-mediated activity against HIV replication and cytotoxicity using MTT assay. The study provided fundamental *in vitro* data supporting the potency of the hexapeptide conjugates and more insights into the applicability of functionalised AuNPs but showed no significant inhibitory activity against HIV (Singh et al., 2019). The antiviral activity of sodium 2-mercaptoethane sulfonate mediated AgNPs (Ag-MES) was determined by testing their ability to inhibit HIV and HSV-1 replication. HIV replication was inhibited more than HSV-1 on the application of the nanorods. Up to 50% of HIV virion growth was inhibited on the application of 5 μg/mL silver nanorods while almost the entire viral cells were inhibited from replication at 10 μmol/mL of the biomaterial. Although the sensitivity was more favoured by the HIV, the nanorods also demonstrated about 90% inhibitory potential against the HSV and thus suggested as a promising antiviral candidate for further study (Fig. 9A) (Etemadzade et al., 2016). Curcumin-stabilized AgNPs were evaluated for antiretroviral efficacy through immunomodulatory activity observed in ACH-2 cells infected latently with the HIV-1 virus. The NPs significantly inhibited the expressions of HIV-1 long terminal repeat (LTR), p24 antigen, interleukin-1β (IL-1β), Tumour necrosis factor-alpha (TNF-αα), IL-6 and nuclear factor-kappa B (NF-kB) by -73% $p < 0.01$, -57% $p < 0.05$, -61% $p < 0.01$, -54% $p < 0.05$, -68% $p < 0.01$ and -79% $p < 0.0001$ respectively. More interestingly, it also inhibited pro-inflammatory responses induced by HIV-1 infection and showed no toxic effect (Sharma et al., 2017). The study supports the therapeutic potency of curcumin-capped AgNPs amenable for translational studies.

5.10. Herpes simplex virus

The infections caused by the Herpes simplex virus (HSV) are human lifelong infections primarily characterized by the periodical reactivation of the viral site of infection. Its transmission occurs predominantly through oral-oral contact and more recently reported oral-genital contact. It causes genital herpes as such categorized among the sexually transmitted infections (STIs) (Donalisio et al., 2020; James et al., 2016) and oftentimes associated with the neurodegenerative disease through deregulation of amyloidogenic and non-amyloidogenic pathways resulting in the aggregation of amyloid-β-peptides (Rodriguez-Izquierdo et al., 2020). In 2016,

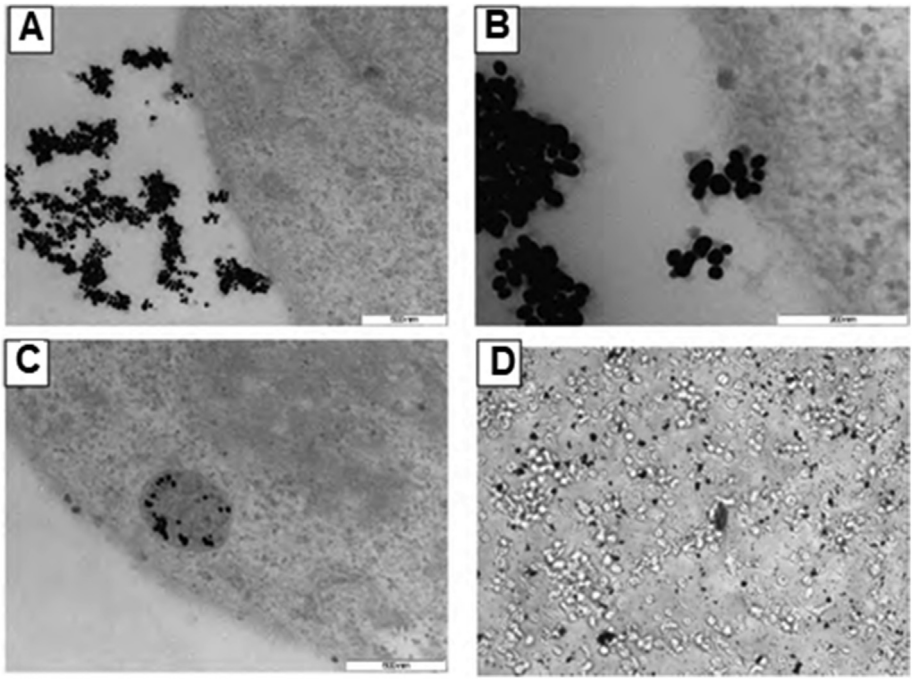

Fig. 8. Electron micrograph of gold NPs show extensive extracellular aggregation (A and B), while only occasional nanoparticles are found within a vesicle in the cytoplasm(C). The aggregates are visible on light microscopy as well (D). (Reproduced from (Parboosing et al., 2018), Licensed under CC BY-NC 4.0).

an estimate of 13.2% of the global population within 15-49-years of age was living with HSV type-2 while the treatment remains difficult (James et al., 2016; Cornell University. Disco, 2019). Green Au and Ag_2O/AgO NPs of *Oscillatoria* sp. *a*nd *Spirulina platensis* were synthesized by El-Sheekh and co-workers, then screened for their antiviral activity against Herpes Simplex virus infection (HSV-1) on Vero cells and evaluated by MTT assay. Up to 90% reduction in CPE of HSV-1 was observed upon application of the NPs each at 31.25 μL/well, although a higher rate (49.23%) was found with the AgNPs over AuNPs (42.75%). The suggested mechanisms of the interesting antiviral activity include glycoprotein agglutination and inhibition of viral infusion into host cells (El-Sheekh et al., 2020). The NPs offer cheaper and easily-accessible therapeutic strategies against HSV infection worthy of further attention.

The HSV infections are sometimes complicated with neurodegenerative diseases. In a recent report, a series of AuNPs labelled NPAuG1-S2, NPAuG2-S4 and NPAuG3-S8 were reportedly screened for antiviral activity against HSV. The NPs were found to possess high antiviral activity against HSV with insignificant toxicity at tested concentrations. The observed mechanisms of their actions include the inhibition of HSV-1 infection in a neural-derived stable transfected SK-N-MC cell and reduction in HSV-1-induced β-amyloid aggregation in SK-APP-D1 (amyloid precursor protein) cell. The NPs demonstrate an ability to cross the blood-brain barrier *in vivo* animal model (Fig. 9B–D) (Rodriguez-Izquierdo et al., 2020), a therapeutic potential for remediating HSV infection in complications with neurodegenerative diseases.

Selvan and co-researchers reportedly prepared some AgNPs of freshwater microalgae, *Neochloris aquatica* and evaluated their antiproliferative and antiviral activities using HeLa and HEp2 cell lines representing cancer and HSV cells respectively. The NPs induced morphological changes, permeabilization of the cell membrane and leakages of cytoplasmic content all leading to cell disruption with IC_{50} of 39.5 and 100 μg/mL for HeLa and Hep2 viral cells respectively (Tamil Selvan et al., 2019). Similarly, biosynthesized AgNPs and *Melaleuca alternifolia* were screened for their activity against HSV-1 and HSV-2. The NPs showed strong antiviral activity against the two viruses with a reduction in CPE by 44.0% and 45.04% for HSV-1 and HSV-2 respectively. Although the mechanisms of actions could not be accurately recorded for the NPs, binding of NPs to viral envelope glycoprotein to inhibit viral-host cell infusion, apoptotic-induced interactions with viral RNA and DNA, and inhibition of viral replication were suggested (Ramadan et al., 2020).

Silver NPs of Tannic acid (TA-AgNPs) was assessed for potential to activate an immune response in vaginal HSV-2-infected mice. The NPs demonstrated interesting antiviral activity *in vivo*, indicated by low viral titres and improved clinical scores earnestly in the animals. The improved immune response was mechanistically observed in terms of an increase in interferon-gamma (IFNγ)+/effector-memory CD8+ T cells (T lymphocytes), activation of plasma cells, B cells (B lymphocytes) and natural killer (NK) cells. These significantly occurred in the TA-AgNP-treated mice compared to the NaCl-treated and control groups (Fig. 10A–F) (Orłowski et al., 2018).

Significant activity was recorded for the AgNPs synthesized by Haggag et al. against HSV-1, HAV-10 and Coxsackie B4 viruses upon evaluation using MTT and metabolome assays. The starting materials showed no antiviral activity against the viruses with the exception being AgNO3 which exhibited activity against HSV-1 with IC50 of 5.13 μg/mL. Hexane extract of *Lampranthus coccineus* exhibited higher efficacy than *Malephora lutea* against HAV-10 virus, HSV-1, Coxsackie B4 virus with IC_{50} value of 11.71 μg/mL, 36.36 μg/mL and 12.74 μg/mL respectively. The aqueous nano extract of *L. coccineus* showed no antiviral activity against HAV-10 and Coxsackie B4 viruses and only a week activity against HSV-1 with IC_{50} of 520 μg/mL (Haggag et al., 2019). The shreds of evidence retrieved from experimental investigations support the therapeutic potentials of Au and Ag NPs (mostly of natural products) against HSV infection and their worthiness for further pharmaceutical development.

5.11. Hepatitis C virus

Hepatitis C virus remains an earmarked health challenge globally through the hepatitis disease due to its virulent action primarily on the liver, complications, resistance and limited treatment options despite concerted scientific strategies (Shady et al., 2020). Generally, symptoms of acute HCV infection are mild and vague, however, it becomes chronic leading to liver damage, cirrhosis and hepatocellular carcinoma when left

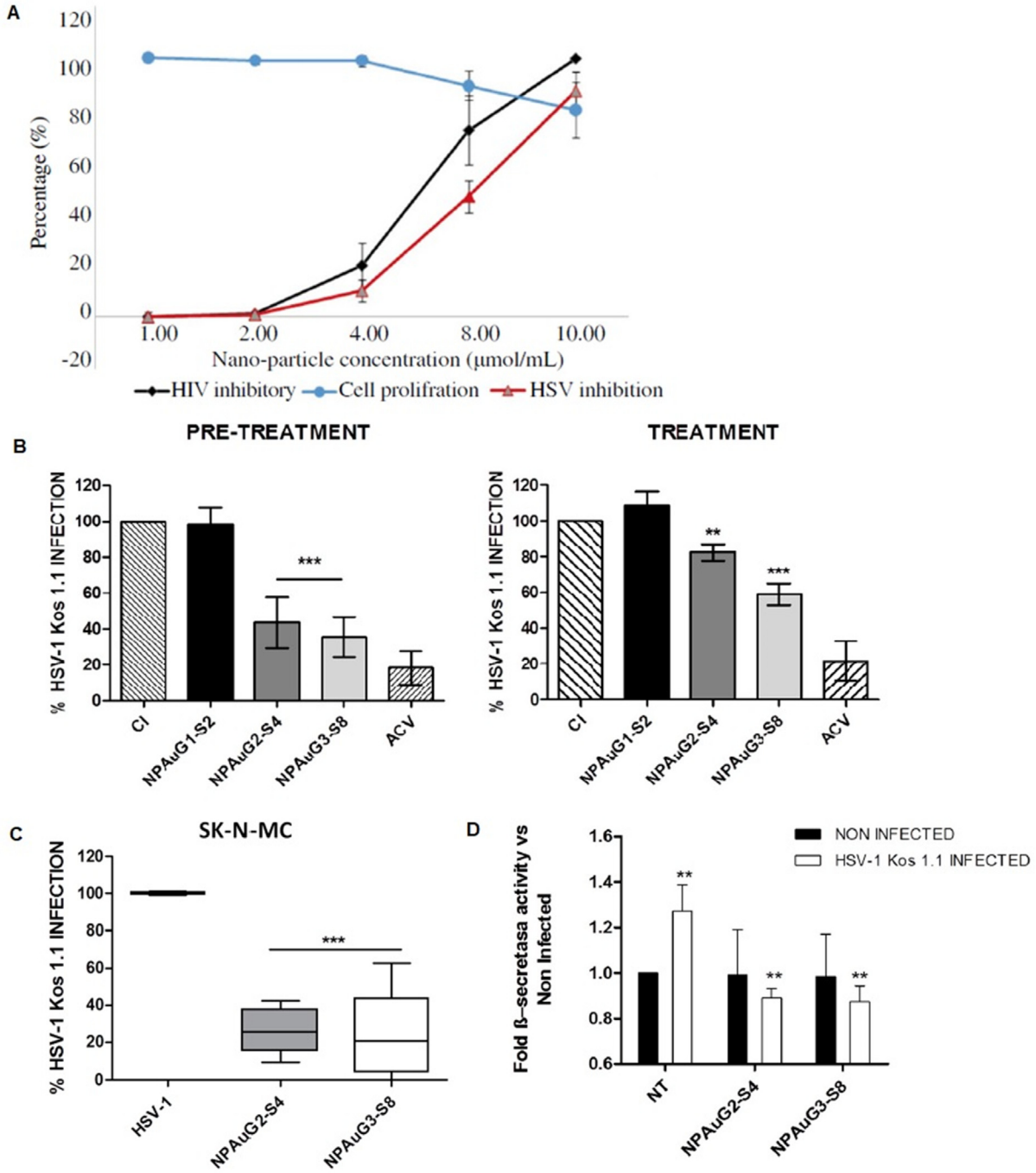

Fig. 9. Antiviral activities of some Au and Ag nanoparticles on HSV. (A) Antiviral activity of sodium 2-mercaptoethan sulfonate on HeLa cells conjugated silver nanorods were shown against HIV and HSV-1 viruses. In this figure, almost entire viral replication was inhibited at 10 μmol/mL. However, HIV showed more sensitivity to synthesized nanorods. (Reproduced with permission from (Etemadzade et al., 2016), copyright (2016) Elsevier (Singapore) Pte Ltd.). (B) Inhibition of HSV-1 infection by NPAus in SK-N-MC cell lines exposed to maximum non-toxic concentrations of the NPs and HSV-1 infected at MOI 1 for 24 h in pre-treatment assay or 1 h in treatment assay. 20 μM ACV was used as a positive control of HSV-1 infection. Data represent mean ± SD from at least three independent experiments performed by duplicate. **; $p < 0.01$; ***; $p < 0.001$. Cl: HSV-1 infection at MOI 1. (C) Cellular protection mediated by NPAus. SK-N-MC cell line was exposed to the maximum non-toxic concentration for 1 h. SK-N-MC cells were washed to eliminate the NPs and infected at MOI 1 for 1 h. Data represent median and interquartile range ±SD from three independent experiments performed by duplicate. ***; $p < 0.001$; HSV-1 infection control at MOI 1. (D) Levels of β-secretase activity in the SK-APP-D1 cell line. SK-APP-D1 cells were treated with NPAus, or NPAus infected with HSV-1. Data represent mean ± SD of three independent experiments performed by triplicate. **; $p < 0.01$; NT: SK-APP-D1 cells. Statistical analysis vs SK-APP-D1 non-treated control cells (Fig. B–D reproduced from (Rodriguez-Izquierdo et al., 2020), Licensed under CC BY 4.0).

untreated. Prevention of severe complications from HCV can be achieved by early detection and treatment of the infection (Ellah et al., 2019). Some AgNPs of total and petroleum ether extracts of *Amphimedon* were evaluated *in vitro* against HCV NS3 helicase and protease activity. The AgNPs of petroleum ether fraction showed more activity against the NS3 helicase IC_{50} value of 0.11 ± 0.62 compared to AgNPs of total extract, $AgNO_3$ and ribavirin whose values are recorded as 1.52 ± 1.18, 77.72 ± and 4.66 ± 0.29 respectively. Similarly, against the NS3 protease, the AgNPs of

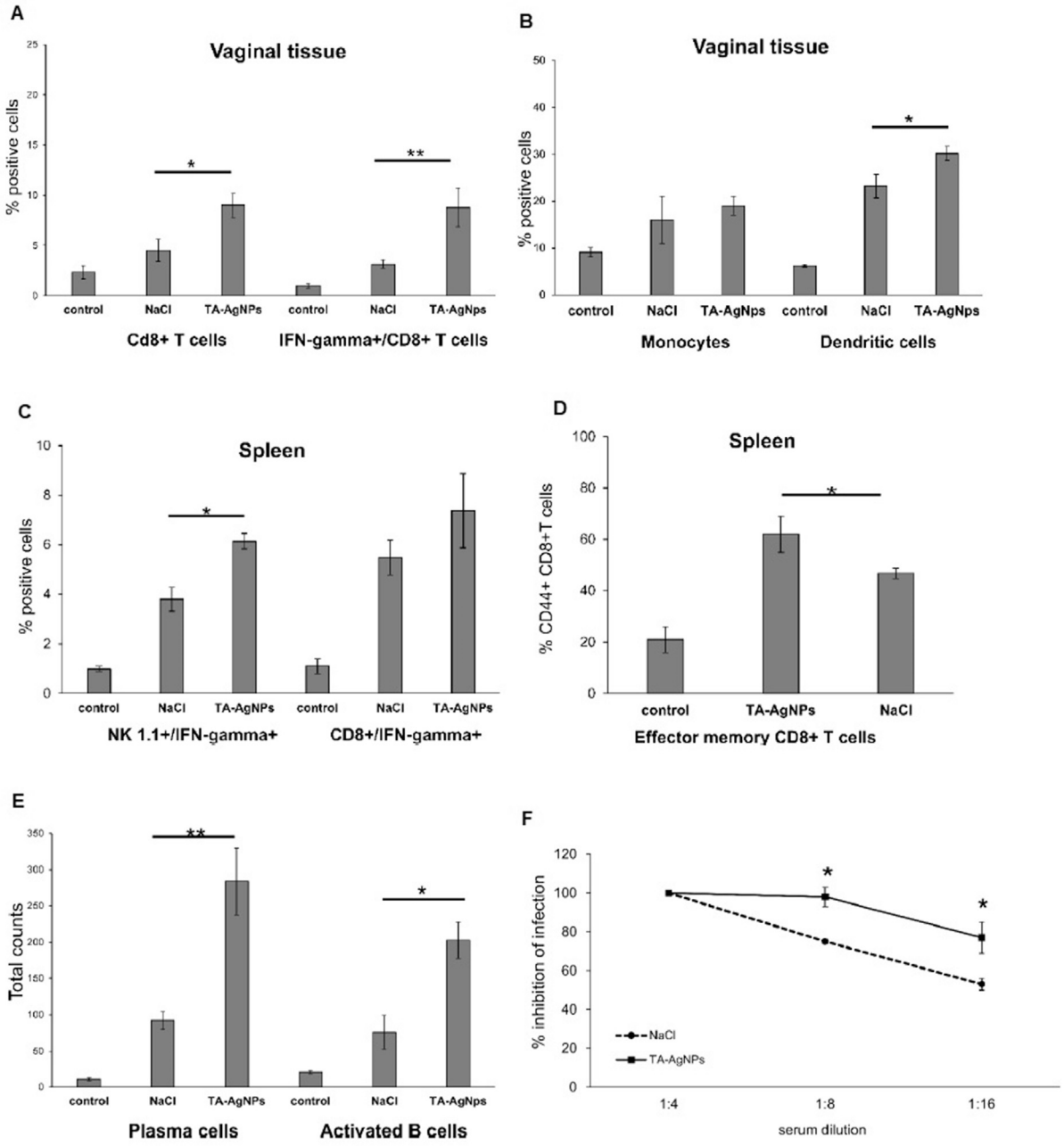

Fig. 10. Treatment with TA-AgNPs helps to boost T, NK and B cells' response and seroneutralization titers after re-challenge. C57BL6 mice were infected intravaginally with HSV-2, then treated with 5 μg/mouse of TA-AgNPs 6, 24, and 48 h after infection. Thirty days later, the mice were re-challenged with the same virus dose. The cell suspensions from the vaginal tissues and spleens were prepared 10 days after re-challenge. The percentage of CD8+ T cells and CD8+/IFNγ+ T cells (A), and monocytes and dendritic cells (B) in the vaginal tissue, as well as the percentage of NK1.1/IFN-gamma+ cells and CD8+/IFN-gamma+ T cells (C), and the effector memory CD8+ T cells (D), were accessed by flow cytometry. (E) The cell suspensions from the vaginal tissues prepared 10 days after re-challenge with HSV-2 were stained for plasma B cells (CD138+/B220low+/IgD) and activated B cells (CD27+/B220+/IgD+). (F) Intravaginal treatment with TA-AgNPs of HSV-2 infection induces better seroneutralization titers. The C57BL6 mice were infected intravaginally with HSV-2 and treated with 5 _g/mouse of TA-AgNPs, then re-challenged thirty days later with the same virus dose. Sera were taken at 10 days after re-challenge with HSV-2 and were subjected to seroneutralization tests. The means are expressed as mean ± SEM for n = 20; * represents significant differences with $p \leq 0.05$, while ** means $p \leq 0.01$. (Reproduced from (Orłowski et al., 2018), Licensed under CC BY 4.0).

petroleum represents the most potent inhibitor with IC_{50} of 2.38 ± 0.57 μg/mL compared to other agents including the drug controls whose IC_{50} values were in the range of 4.77 ± 0.26–52.67 ± 0.33 μg/mL (Shady et al., 2020). Although the mechanisms of activity remain understudied, the AgNPs of petroleum extract of *Amphimedon* demonstrated promising efficacy against HCV, worthy of further translational study.

5.12. Dengue

Dengue virus (DEN-2) is an arthropod-borne, single positive-stranded RNA virus with renowned transmission within the tropical and subtropical regions of the world through *Aedes aegypti,* its primary mosquito vector which spreads the disease during blood-feeding (Murugan et al.,

2015). No specific treatment has been identified for the virulent disease, as such most effective strategy has been focused on prevention through the control of its vector (Sujitha et al., 2015; Murugan et al., 2015). Recently, some AuNPs demonstrated a size-dependent neutralising potentials on the dengue virus and as such suggested for further translational design into DEN-2 vaccine (Quach et al., 2018). Series of nanobiomaterials have been prepared with prophylaxis and treatment potentials against the deadly disease. Biosynthesized AgNPs of *Moringa oleifera* seed extract exhibited *in vitro* antiviral activity against DEN-2, reducing the viral titer loads quantitatively from 7 $\log_{10}$ in AgNP-free control to 3.8 $\log_{10}$ $TCID_{50}$/mL after a single treatment with 20 μL/mL of the NPs. The yield of DEN-2 in the control became 5.8 $\log_{10}$ PFU/mL while it remained 1.4 $\log_{10}$ PFU/mL 6 h after treatment with 20 μL/mL of the NPs. High efficacy of the nanoparticle was recorded against its major vector, *A. aegypti* with LC_{50} of 10.24–21.17 ppm for I instar larvae and pupae respectively (Sujitha et al., 2015) Results from RT-PCR antiviral evaluation of AgNPs of *Bruguiera cylindrical* indicated significant inhibition of dengue virus envelope protein and downregulation of the viral E gene after treatment with 30 μg/mL dose. The NPs demonstrate high cytotoxicity against the viral cells with LC_{50} values of 8.935, 11.028, 13.913, 22.443 and 30.698 ppm for I instar, II instar, III instar, IV instar and pupa respectively. A decline of 35% was observed in Vero cell viability on exposure to 30 μg/mL of AgNP for 24 h. More interestingly, the NPs show no effect on the predation efficiency of goldfish (*Carassius auratus*) against *A. aegypti* at sub-lethal doses, indicating its insignificance on non-targets (Murugan et al., 2015). The evidence supports the propensity of the AgNPs of *Moringa oleifera* seed and *Bruguiera cylindrical* leaves on vector-dependent prevention of dengue viral infection worthy of further evaluation.

5.13. Poliovirus

Polio (Poliomyelitis) is a contagious paralytic/disabling disease caused by the poliovirus. It's mostly characterized by non-visible symptoms, commonly affecting children and usually prevented through vaccination (hat is Polio. Cente, 2020). Some silver nanobiomaterials were reportedly synthesised *via* the electrochemical method and evaluated *in vitro* for therapeutic potential against the virus using inverted light microscopy. Various concentrations of the NPs were added to 96 well plates containing human rhabdomyosarcoma (RD) cells before incubation with poliovirus. The cell viability of the synthesised AgNPs was 90%, 87% and 83% at 24, 48 and 72 h respectively. This showed high viability and low cytotoxicity against the RD cells. The NPs were screened against polioviruses where the antiviral activities were found at 3.13 ppm, corresponding to 1$TCID_{50}$ and 10 $TCID_{50}$ after 30 and 60 min respectively of incubation with poliovirus. The cell viability of up to 98% was recorded after 48 h of treatment with no significant CPE (Huy et al., 2017), indicating the disinfecting potentials of the electrochemically synthesised AgNP against poliovirus.

5.14. Enterovirus

Enterovirus 17 (EV71) is identified with some neurological diseases, and hand, foot and mouth disease (HFMD) especially in children, while effective therapeutic options remain challenging. Small interfering RNAs are potential anti-EV71, however, the inability to cross cell membranes limits their application. Thus, modification through nanotechnology is ideally targeted for enhancing their transfection, taking advantage of promising antiviral activities of AgNPs. Consequently, the protective ability of surface decorated AgNPs of PEI and siRNA, PEI and siRNA was assessed via MTT assay and cytotoxic effects of enterovirus 71(EV71) virus on Vero cells. Vero cells showed the viability of 25% on treatment with EV71 virus, which was increased to 40% and 62% on treating with AgNPs and AgNPs of PEI respectively. There was a massive increase in cell viability on treating with AgNPs of PEI and siRNA, recording 85% cell viability. Change in morphology, loss of cell-to-cell contact and reduction in cell numbers resulted from the infection of Vero cells with EV71 virus. The introduction of AgNPs of PEI and siRNA led to a reduction of the effect of the virus, making the cells appear healthy and regular in shape. The multi-mechanistic pharmacology of the nanocomposites is hypothesized as the blocking of EV71 cell infusion, prevention of DNA fragmentation, inhibition of ROS accumulation, chromatin condensation and activations of caspase-3, AKT and P53 (Li et al., 2017). Although, further investigational studies, especially *in vivo* animal models are required to validate the real-life observation of the pharmaco-physiological effects. Similarly, the effective experimental results of some golden-star nanoparticles in animal model by Teng and co-workers led to the suggestion of the nanobiomaterials as adjuvants and immunoprotective agents against HFMD, subject to further evaluation (Teng et al., 2018).

5.15. Rift Valley fever virus

Borrego et al. screened Argovit for antiviral activity against Rift Valley fever virus (RVFV) on Vero cell cultures. The NPs showed limited activity when applied post-infection, while they showed higher activity against the infection when applied pre-infection. Incubating 12 μg/mL of Argovit with the virus leads to a 98% reduction in infection while 60% inhibition was recorded on inoculation with 1.2 μg/mL (Borrego et al., 2016). Progressively, some AuNPs were demonstrated to induce immunohistochemical and histological changes in rat spleen, as such, suggested for further studies as potential adjuvant vaccine against the RVFV (Soliman et al., 2017).

6. Gold and silver nanoparticles in virus detection

Several NPs of Au and Ag have been reported with potentials for viral diagnosis through testing and detection within living and non-living entities with sensitivity depending on the natures of the NP cores (Draz and Shafiee, 2018). Consequently, various respiratory viruses with a proclivity for a pandemic such as the influenza virus, SARS-CoVs and MERS-CoV have been reportedly detected using nanobiosensors, most of which are DNA- or antibody-dependent with an electrochemical, field-effect transistor or optical transduction (Alhalaili et al., 2019; Antiochia, 2020). For instance, double-stranded DNA, MERS-CoV was experimentally detected through label-free colourimetric assay incorporating self-assembly shielded AuNP in the presence of positive electrolytes. The viral presence was verified using localized SPR, (LSPR) (Kim et al., 2019), supporting the extended applications of AuNP as a biosensor.

7. Conclusion and future perspectives

Nanotechnology has aided the design of functionalised and non-functionalised Au and Ag nanobiomaterials through physical, chemical and biological (green synthesis) methods. In this review, the innovative designs as well as interesting antiviral activities of the nanotechnology-inclined biomaterials of Au and Ag, reported in the last 5 years were critically overviewed to identify promising candidates against several viral diseases affecting man. These include influenza, respiratory syncytial, adenovirus, severe acute respiratory syndromes, rotavirus, norovirus, measles, chikungunya, HIV, herpes simplex virus, dengue, polio, enterovirus and rift valley fever virus.

Notably, a nanotechnologically designed **AuNP-M2e peptide vaccine**, **AgNP of cinnamon bark extract** and **AgNP of oseltamivir** are promising candidates against influenza. **A PVP-coated AgNP** displayed potency for drug design against RSV, a viral infection commonly affecting children with no specific therapeutic option. Against the current SARS-CoV-2, **PVP-AgNPs** of ≈10 nm inhibited the viral entry through the disruption of viral integrity while **AuNRs of a peptide pregnancy-induced hypertension** and **AuNP nanocarriers of antigen** were effective inhibitors against MERS-CoV and SARS-CoV respectively. The **AgNPs of collagen and *B. subtilis*** were impressively active against rotavirus, although with some cytotoxicity concern at high temperatures.

As a potential application for water disinfection, **AgNPs labelled Ag30–SiO_2** demonstrated a strong antiviral activity against murine norovirus in water. Similarly, **AuNPs of *Allium sativum*** and **AgNPs of ribavirin** displayed better efficacy than ribavirin against measles by enhancing the activity and delivery of the antiviral agents to targets. The **AgNPs of *C. limetta*** and ***A. paniculata*** showed interesting virucidal potentials against Chikungunya, as such, worthy of further investigation. Interestingly, **AuNPs of efavirenz** and **stavudine** demonstrated better delivery to target and inhibition of HIV compared to respective drugs while **AgNPs-curcumin** inhibited the pro-inflammation responses induced by HIV with no toxic effect. Oftentimes, the HSV is reportedly complicated with neurodegenerative diseases involving the Aβ peptide aggregation. A gold NP of the oligonucleotide, **NPAuG3-S8** displayed potent virucidal activity and interestingly crossed the blood-brain barrier in a mice model, indicating a potential for HSV associated with neurodegenerative diseases for further investigation. The **AgNPs of *M. oleifera*** and ***B. cylindrical*** are promising candidates for future studies against dengue-inducing *Aedes aegypti*, while **AgNPs** of **polyethyleneimine** and **siRNA** analogues were potent against enterovirus, neurological disease and commonly affecting the foot, hand and mouth especially in children.

The interesting activities of the highlighted nanoparticle analogues were recorded through multi-mechanistic pharmacology, involving most implicated biological targets in viral infections. This indicates their promising potentials to overcome drug resistance challenges usually associated with prophylaxis and treatment of viral disease. Moreover, their designs into nano-sizes favour effective delivery to therapeutic target cells in active doses. Advantageously, more of the preparation procedure was achieved through the cheaper and environmentally safer biological methods (green synthesis). However, in most reported cases, crude extracts were used, making the proposal of mechanisms of antiviral activities through the molecular interactions with therapeutic targets difficult. Future scientific exploration could be focused on the application of pure phytochemical isolates for the synthesis (unicapping) of the NPs. As such, a plausible mechanism of action would be succinctly demonstrated in a structure-activity relationship (SAR). Naturally occurring phytochemicals with good synthetic accessibility and diverse biological activities such as β-carboline alkaloids could provide a good unicapping opportunity for improved design of Au and Ag NPs with more interesting antiviral pharmacology. Despite the interesting antiviral pharmacology of the overviewed NPs, their cytotoxicity to normal cells was less evaluated. This should importantly form the basis for further studies, especially considering the nanosize and elemental natures of Au and Ag which are of serious scientific debates in terms of biocompatibility. Most of the activity evaluation protocols were recorded through *in vitro* models in which the physiological side effects could not be adequately observed. As such, future studies on the highlighted NPs are recommended through *in vivo* experimental models to evaluate their expressions for toxicity and side effects. In summary, this review represents a model for an efficient design of nanobiomaterials and identifies promising candidates recommended for further translational studies towards therapeutic designs for the prevention and treatment of human viral diseases.

Declaration of competing interest

The authors declare that they have no known competing financial interests or personal relationships that could have appeared to influence the work reported in this paper.

Acknowledgement

This work was financially supported by the Fundamental Research Grant Scheme, Ministry of Higher Education, Malaysia, HICoE (grant no. 203.CDADAH.6711955). YOA is grateful to the Tertiary Education Fund Nigeria for PhD scholarship and Universiti Sains Malaysia for Graduate Assistant Scheme (grant no. 308.AIPS.415401).

References

Abdulla, L., Alshehddi, A., Bokhari, N., 2020. Saudi Journal of Biological Sciences Influence of gold and silver nanoparticles on the germination and growth of Mimusops laurifolia seeds in the South-Western regions in Saudi Arabia. Saudi J. Biol. Sci. 27, 574–580. https://doi.org/10.1016/j.sjbs.2019.11.013.

Ahmad, F., Ashraf, N., Ashraf, T., Zhou, R.-B., Yin, D.-C., 2019. Biological synthesis of metallic nanoparticles (MNPs) by plants and microbes: their cellular uptake, biocompatibility, and biomedical applications. Appl. Microbiol. Biotechnol. https://doi.org/10.1007/s00253-019-09675-5.

Ahmed, E.M., Solyman, S.M., Mohamed, N., Boseila, A.A., Hanora, A.S., 2018. Antiviral activity of Ribavirin nano-particles against measles virus. Cell. Mol. Biol. 64, 24–32. https://doi.org/10.14715/cmb/2018.64.9.4.

Akbarzadeh, A., Kafshdooz, L., Razban, Z., Dastranj Tbrizi, A., Rasoulpour, S., Khalilov, R., et al., 2018. An overview application of silver nanoparticles in inhibition of herpes simplex virus. Artif. Cells Nanomed. Biotechnol. 46, 263–267. https://doi.org/10.1080/21691401.2017.1307208.

Alghrair, Z.K., Fernig, D.G., Ebrahimi, B., 2019. Enhanced inhibition of influenza virus infection by peptide-noble-metal nanoparticle conjugates. Beilstein J. Nanotechnol. 10, 1038–1047. https://doi.org/10.3762/BJNANO.10.104.

Alhalaili, B., Popescu, I.N., Kamoun, O., Alzubi, F., Alawadhia, S., Vidu, R., 2019. Nanobiosensors for the detection of novel coronavirus 2019-nCoV and other pandemic/epidemic respiratory viruses: a review. Sensors 20, 6591. https://doi.org/10.3390/s20226591.

Antiochia, R., 2020. Nanobiosensors as new diagnostic tools for SARS, MERS and COVID-19: from past to perspectives. Microchim. Acta 187. https://doi.org/10.1007/s00604-020-04615-x.

Avilala, J., Golla, N., 2019. Antibacterial and antiviral properties of silver nanoparticles synthesized by marine actinomycetes. Int. J. Pharm. Sci. Res. 10, 1223–1228. https://doi.org/10.13040/IJPSR.0975-8232.10(3, 1223-28.

Ayipo, Y.O., Osunniran, W.A., Mordi, M.N., 2021. Metal complexes of β-carboline: advances in anticancer therapeutics. Coord. Chem. Rev. 432, 213746. https://doi.org/10.1016/j.ccr.2020.213746.

Ayipo, Y.O., Mordi, M.N., Mustapha, M., Damodaran, T., 2021. Neuropharmacological potentials of β-carboline alkaloids for neuropsychiatric disorders. Eur. J. Pharmacol. 893, 173837. https://doi.org/10.1016/j.ejphar.2020.173837.

Babaei, A., Mousavi, S.M., Ghasemi, M., Pirbonyeh, N., Soleimani, M., Moattari, A., 2021. Gold nanoparticles show potential in vitro antiviral and anticancer activity. Life Sci. 284, 119652. https://doi.org/10.1016/j.lfs.2021.119652.

Badeggi, U.M., Lawal, B.A., Akinfenwa, A.O., Ayipo, Y.O., Azeh, Y., Dagaci, M.Z., 2020. Physicochemical properties and in vitro stability studies of green synthesized gold nanoparticles using pelargonium sidoides. Niger. J. Technol. 39, 785–791. https://doi.org/10.4314/njt.v39i3.18.

Badeggi, U.M., Badmus, J.A., Botha, S.S., Ismail, E., Marnewick, J.L., Africa, C.W.J., et al., 2020. Biosynthesis, characterization, and biological activities of procyanidin capped silver nanoparticles. J. Funct. Biomater. 11, 1–20. https://doi.org/10.3390/JFB11030066.

Badeggi, U.M., Ismail, E., Adeloye, A.O., Botha, S., Badmus, J.A., Marnewick, J.L., et al., 2020. Green synthesis of gold nanoparticles capped with procyanidins from leucosidea sericea as potential antidiabetic and antioxidant agents. Biomolecules 10. https://doi.org/10.3390/biom10030452.

Borrego, B., Lorenzo, G., Mota-Morales, J.D., Almanza-Reyes, H., Mateos, F., López-Gil, E., et al., 2016. Potential application of silver nanoparticles to control the infectivity of Rift Valley fever virus in vitro and in vivo. Nanomed. Nanotechnol. Biol. Med. 12, 1185–1192. https://doi.org/10.1016/j.nano.2016.01.021.

Campos, E.V.R., Pereira, A.E.S., De Oliveira, J.L., Carvalho, L.B., Guilger-Casagrande, M., De Lima, R., et al., 2020. How can nanotechnology help to combat COVID-19? Opportunities and urgent need. J. Nanobiotechnol. 18, 1–23. https://doi.org/10.1186/s12951-020-00685-4.

CDC, 2020. What is Polio. Centers Dis. Control. Prev. https://www.cdc.gov/polio/what-is-polio/index.htm.

Chen, Y.N., Hsueh, Y.H., Hsieh, C Te, Tzou, D.Y., Chang, P.L., 2016. Antiviral activity of graphene–silver nanocomposites against non-enveloped and enveloped viruses. Int. J. Environ. Res. Public Health 13, 4–6. https://doi.org/10.3390/ijerph13040430.

Choudhary, S., Kumar, R., Dalal, U., Tomar, S., Reddy, S.N., 2020. Green synthesis of nanometal impregnated biomass – antiviral potential. Mater. Sci. Eng. C 112, 110934. https://doi.org/10.1016/j.msec.2020.110934.

Cornell University, 2019. Discovery Reveals Mechanism that Turns Herpes Virus On and Off. ScienceDaily. www.sciencedaily.com/releases/2019/11/191114161905.htm.

Danaei, M., Dehghankhold, M., Ataei, S., Davarani, F.H., Javanmard, R., Dokhani, A., et al., 2018. Impact of particle size and polydispersity index on the clinical applications of lipidic nanocarrier systems. Pharmaceutics 10, 1–17. https://doi.org/10.3390/pharmaceutics10020057.

Donalisio, M., Argenziano, M., Rittà, M., Bastiancich, C., Civra, A., Lembo, D., et al., 2020. Acyclovir-loaded sulfobutyl ether-β-cyclodextrin decorated chitosan nanodroplets for the local treatment of HSV-2 infections. Int. J. Pharm. 587, 119676. https://doi.org/10.1016/j.ijpharm.2020.119676.

Draz, M.S., Shafiee, H., 2018. Applications of gold nanoparticles in virus detection. Theranostics 8, 1985–2017. https://doi.org/10.7150/thno.23856.

Dung, T.T.N., Nam, V.N., Nhan, T.T., Ngoc, T.T.B., Minh, L.Q., Nga, B.T.T., et al., 2019. Silver nanoparticles as potential antiviral agents against African swine fever virus. Mater. Res. Express 6. https://doi.org/10.1088/2053-1591/ab6ad8.

Dykman, L.A., 2020. Gold nanoparticles for preparation of antibodies and vaccines against infectious diseases. Expert Rev. Vaccines 19, 465–477. https://doi.org/10.1080/14760584.2020.1758070.

Elazzazy, A.M., Elbeshehy, E.K.F., Betiha, M.A., 2017. In vitro assessment of activity of graphene silver composite sheets against multidrug-resistant bacteria and Tomato Bushy Stunt Virus. Trop. J. Pharm. Res. 16, 2705–2711. https://doi.org/10.4314/tjpr.v16i11.19.

Elbeshehy, E.K.F., Elazzazy, A.M., Aggelis, G., 2015. Silver nanoparticles synthesis mediated by new isolates of Bacillus spp., nanoparticle characterization and their activity against Bean Yellow Mosaic Virus and human pathogens. Front. Microbiol. 6, 1–13. https://doi.org/10.3389/fmicb.2015.00453.

Ellah, N.H.A., Tawfeek, H.M., John, J., Hetta, H.F., 2019. Nanomedicine as a future therapeutic approach for Hepatitis C virus. Nanomedicine 14, 1471–1491. https://doi.org/10.2217/nnm-2018-0348.

Eggleton, J., Nagalli, S., 2020. Highly Active Antiretroviral Therapy (HAART). Treasure Isl StatPearls Publ. https://www.ncbi.nlm.nih.gov/books/NBK554533/. (Accessed 11 February 2021).

El-Bendary, M.A., Moharam, M.E., Abdelraof, M., Allam, M.A., Roshdy, A.M., Shaheen, M.N.F., et al., 2019. Multi-bioactive silver nanoparticles synthesized using mosquitocidal Bacilli and their characterization. Arch. Microbiol. 202, 63–75. https://doi.org/10.1007/s00203-019-01718-9.

El-Bendary, M.A., Afifi, S.S., Moharam, M.E., Abo El-Ola, S.M., Salama, A., Omara, E.A., et al., 2020. Biosynthesis of silver nanoparticles using isolated Bacillus subtilis: characterization, antimicrobial activity, cytotoxicity, and their performance as antimicrobial agent for textile materials. Prep. Biochem. Biotechnol. 1–15. https://doi.org/10.1080/10826068.2020.1789992, 0.

El-Gaffary, M., Bashandy, M.M., Ahmed, A.R., El-Borady, O.M., 2019. Self-assembled gold nanoparticles for in-vitro inhibition of bovine viral diarrhea virus as surrogate model for HCV. Mater. Res. Express 6. https://doi.org/10.1088/2053-1591/ab18b6.

El-Sheekh, M.M., Shabaan, M.T., Hassan, L., Morsi, H.H., 2020. Antiviral activity of algae biosynthesized silver and gold nanoparticles against Herps Simplex (HSV-1) virus in vitro using cell-line culture technique. Int. J. Environ. Health Res. 1–12. https://doi.org/10.1080/09603123.2020.1789946, 00.

Etemadzade, M., Ghamarypour, A., Zabihollahi, R., shabbak, G., Shirazi, M., Sahebjamee, H., et al., 2016. Synthesis and evaluation of antiviral activities of novel sonochemical silver nanorods against HIV and HSV viruses. Asian Pacific J. Trop. Dis. 6, 854–858. https://doi.org/10.1016/S2222-1808(16)61145-3.

Fatima, M., Zaidi, N. us SS., Amraiz, D., Afzal, F., 2015. In vitro antiviral activity of Cinnamomum cassia and its nanoparticles against H7N3 influenza a virus. J. Microbiol. Biotechnol. 26, 151–159. https://doi.org/10.4014/jmb.1508.08024.

Fawzy, M., Khairy, G.M., Hesham, A., Rabaan, A.A., El-Shamy, A.G., Nagy, A., 2021. Nanoparticles as a novel and promising antiviral platform in veterinary medicine. Arch. Virol. 166, 2673–2682. https://doi.org/10.1007/s00705-021-05177-w.

García-Serradilla, M., Risco, C., Pacheco, B., 2019. Drug repurposing for new, efficient, broad spectrum antivirals. Virus Res. 264, 22–31. https://doi.org/10.1016/j.virusres.2019.02.011.

Ghaffari, E., Rezatofighi, S.E., Ardakani, M.R., Rastegarzadeh, S., 2019. Delivery of antisense peptide nucleic acid by gold nanoparticles for the inhibition of virus replication. Nanomedicine 14, 1827–1840. https://doi.org/10.2217/nnm-2018-0520.

Gianvincenzo, P Di, Calvo, J., Perez, S., Álvarez, A., Bedoya, L.M., Alcamí, J., et al., 2015. Negatively charged glyconanoparticles modulate and stabilize the secondary structures of a gp120 V3 loop peptide: toward fully synthetic HIV vaccine candidates. Bioconjug. Chem. 26, 755–765. https://doi.org/10.1021/acs.bioconjchem.5b00077.

Govindappa, M., Hemashekhar, B., Arthikala, M.K., Rai, V.R., Ramachandra, Y.L., 2018. Characterization, antibacterial, antioxidant, antidiabetic, anti-inflammatory and antityrosinase activity of green synthesized silver nanoparticles using Calophyllum tomentosum leaves extract. Results Phys. https://doi.org/10.1016/j.rinp.2018.02.049.

Haggag, E.G., Elshamy, A.M., Rabeh, M.A., Gabr, N.M., Salem, M., Youssif, K.A., et al., 2019. Antiviral potential of green synthesized silver nanoparticles of lampranthus coccineus and malephora lutea. Int. J. Nanomed. 14, 6217–6229. https://doi.org/10.2147/IJN.S214171.

Huang, X., Li, M., Xu, Y., Zhang, J., Meng, X., An, X., et al., 2019. Novel gold nanorod-based HR1 peptide inhibitor for Middle East respiratory syndrome coronavirus. ACS Appl. Mater. Interfaces 11, 19799–19807. https://doi.org/10.1021/acsami.9b04240.

Huy, T.Q., Hien Thanh, N.T., Thuy, N.T., Chung, P Van, Hung, P.N., Le, A.T., et al., 2017. Cytotoxicity and antiviral activity of electrochemical – synthesized silver nanoparticles against poliovirus. J. Virol. Methods 241, 52–57. https://doi.org/10.1016/j.jviromet.2016.12.015.

Ibrahim, S., Ahmad, Z., Manzoor, M.Z., Mujahid, M., Faheem, Z., Adnan, A., 2021. Optimization for biogenic microbial synthesis of silver nanoparticles through response surface methodology , characterization , their antimicrobial , antioxidant , and catalytic potential. Sci. Rep. 1–18. https://doi.org/10.1038/s41598-020-80805-0.

Ijaz, I., Gilani, E., Nazir, A., Bukhari, A., 2020. Detail review on chemical, physical and green synthesis, classification, characterizations and applications of nanoparticles. Green Chem. Lett. Rev. 13, 59–81. https://doi.org/10.1080/17518253.2020.1802517.

James, C., Harfouche, M., Welton, N.J., Turner, K.M.E., Abu-Raddad, L.J., Gottlieb, S.L., et al., 2020. Herpes simplex virus: global infection prevalence and incidence estimates, 2016. Bull. World Health Organ. 98, 315–329. https://doi.org/10.2471/BLT.19.237149.

Javaid, A., Oloketuyi, S.F., Khan, M.M., Khan, F., 2018. Diversity of bacterial synthesis of silver nanoparticles. Bionanoscience 8, 43–59. https://doi.org/10.1007/s12668-017-0496-x.

Jeremiah, S.S., Miyakawa, K., Morita, T., Yamaoka, Y., Ryo, A., 2020. Potent antiviral effect of silver nanoparticles on SARS-CoV-2. Biochem. Biophys. Res. Commun. 533, 195–200. https://doi.org/10.1016/j.bbrc.2020.09.018.

Joe, Y.H., Park, D.H., Hwang, J., 2016. Evaluation of Ag nanoparticle coated air filter against aerosolized virus: anti-viral efficiency with dust loading. J. Hazard Mater. 301, 547–553. https://doi.org/10.1016/j.jhazmat.2015.09.017.

Kaushik, S., Sharma, V., Chhikara, S., Yadav, J.P., Kaushik, S., 2019. Anti-chikungunya activity of green synthesized silver nanoparticles using Carica Papaya leaves in animal cell culture model. Asian J. Pharm. Clin. Res. 12, 170–174. https://doi.org/10.22159/ajpcr.2019.v12i6.32179.

Khan, A.U., Malik, N., Khan, M., Cho, M.H., Khan, M.M., 2018. Fungi-assisted silver nanoparticle synthesis and their applications. Bioprocess Biosyst. Eng. 41. https://doi.org/10.1007/s00449-017-1846-3.

Khoobchandani, M., Katti, K.K., Karikachery, A.R., Thipe, V.C., Srisrimal, D., Darshakumar, R.D., 2020. New approaches in breast cancer therapy through green nanotechnology and nano-ayurvedic medicine – pre-clinical and pilot human clinical investigations. Int. J. Nanomed. 15, 181–197.

Kim, H., Park, M., Hwang, J., Kim, J.H., Chung, D.R., Lee, K Sung, et al., 2019. Development of label-free colorimetric assay for MERS-CoV using gold nanoparticles. ACS Sens. 4, 1306–1312. https://doi.org/10.1021/acssensors.9b00175.

Kumari, S., Chatterjee, K., 2021. Biomaterials-based formulations and surfaces to combat viral infectious diseases. APL Bioeng. 5. https://doi.org/10.1063/5.0029486.

Lakshminarayanan, R., Ye, E., Young, D.J., Li, Z., Loh, X.J., 2018. Recent advances in the development of antimicrobial nanoparticles for combating resistant pathogens. Adv. Healthc. Mater. 7, 1–13. https://doi.org/10.1002/adhm.201701400.

Li, Y., Lin, Z., Zhao, M., Guo, M., Xu, T., Wang, C., et al., 2016. Reversal of H1N1 influenza virus-induced apoptosis by silver nanoparticles functionalized with amantadine. RSC Adv. 6, 89679–89686. https://doi.org/10.1039/c6ra18493f.

Li, Y., Lin, Z., Zhao, M., Xu, T., Wang, C., Hua, L., et al., 2016. Silver nanoparticle based codelivery of oseltamivir to inhibit the activity of the H1N1 influenza virus through ROS-mediated signaling pathways. ACS Appl. Mater. Interfaces 8, 24385–24393. https://doi.org/10.1021/acsami.6b06613.

Li, Y., Lin, Z., Xu, T., Wang, C., Zhao, M., Xiao, M., et al., 2017. Delivery of VP1 siRNA to inhibit the EV71 virus using functionalized silver nanoparticles through ROS-mediated signaling pathways. RSC Adv. 7, 1453–1463. https://doi.org/10.1039/c6ra26472g.

Li, Y., Xiao, Y., Chen, Y., Huang, K., 2021. Nano-based approaches in the development of antiviral agents and vaccines. Life Sci. 265, 118761. https://doi.org/10.1016/j.lfs.2020.118761.

Lysenko, V., Lozovski, V., Lokshyn, M., Gomeniuk, Y.V., Dorovskih, A., Rusinchuk, N., et al., 2018. Nanoparticles as antiviral agents against adenoviruses. Adv. Nat. Sci. Nanosci. Nanotechnol. 9. https://doi.org/10.1088/2043-6254/aac42a.

Maduray, K., Parboosing, R., 2020. Metal nanoparticles: a promising treatment for viral and arboviral infections. Biol. Trace Elem. Res. https://doi.org/10.1007/s12011-020-02414-2.

Malik, T., Chauhan, G., Rath, G., Kesarkar, R.N., Chowdhary, A.S., Goyal, A.K., 2018. Efaverinz and nano-gold-loaded mannosylated niosomes: a host cell-targeted topical HIV-1 prophylaxis via thermogel system. Artif. Cells Nanomed. Biotechnol. 46, 79–90. https://doi.org/10.1080/21691401.2017.1414054.

Medhi, R., Srinoi, P., Ngo, N., Tran, H.V., Lee, T.R., 2020. Nanoparticle-based strategies to combat COVID-19. ACS Appl. Nano Mater. 3, 8557–8580. https://doi.org/10.1021/acsanm.0c01978.

Mehranfar, A., Izadyar, M., 2020. Theoretical design of functionalized gold nanoparticles as antiviral agents against severe acute respiratory syndrome coronavirus 2 (SARS-CoV-2). J. Phys. Chem. Lett. 2, 10284–10289. https://doi.org/10.1021/acs.jpclett.0c02677.

Meléndez-Villanueva, M.A., Morán-Santibañez, K., Martínez-Sanmiguel, J.J., Rangel-López, R., Garza-Navarro, M.A., Rodríguez-Padilla, C., et al., 2019. Virucidal activity of gold nanoparticles synthesized by green chemistry using garlic extract. Viruses 11, 1–13. https://doi.org/10.3390/v11121111.

Morris, D., Ansar, M., Speshock, J., Ivanciuc, T., Qu, Y., Casola, A., et al., 2019. Antiviral and immunomodulatory activity of silver nanoparticles in experimental rsv infection. Viruses 11. https://doi.org/10.3390/v11080732.

Murphy, M., Ting, K., Zhang, X., Soo, C., Zheng, Z., 2015. Current development of silver nanoparticle preparation , investigation , and application in the field of medicine. J. Nanomater. 2015, 1–12. https://doi.org/10.1155/2015/696918.

Murugan, K., Dinesh, D., Paulpandi, M., Althbyani, A.D.M., Subramaniam, J., Madhiyazhagan, P., et al., 2015. Nanoparticles in the fight against mosquito-borne diseases: bioactivity of Bruguiera cylindrica-synthesized nanoparticles against dengue virus DEN-2 (in vitro) and its mosquito vector Aedes aegypti (Diptera: Culicidae). Parasitol. Res. 114, 4349–4361. https://doi.org/10.1007/s00436-015-4676-8.

Orłowski, P., Kowalczyk, A., Tomaszewska, E., Ranoszek-Soliwoda, K., Węgrzyn, A., Grzesiak, J., et al., 2018. Antiviral activity of tannic acid modified silver nanoparticles: potential to activate immune response in herpes genitalis. Viruses 10, 1–15. https://doi.org/10.3390/v10100524.

Palmieri, V., Papi, M., 2020. Can graphene take part in the fight against COVID-19? Nano Today 33, 100883. https://doi.org/10.1016/j.nantod.2020.100883.

Parboosing, R., Govender, T., Maguire, G.E.M., Kruger, H.G., 2018. Synthesis, characterization and biocompatibility of a multifunctional gold nanoparticle system for the delivery of single-stranded RNA to lymphocytes. South African J. Chem. 71, 1–14. https://doi.org/10.17159/0379-4350/2018/v71a1.

Park, S.J., Ko, Y.S., Jung, H., Lee, C., Woo, K., Ko, G.P., 2018. Disinfection of waterborne viruses using silver nanoparticle-decorated silica hybrid composites in water environments. Sci. Total Environ. 625, 477–485. https://doi.org/10.1016/j.scitotenv.2017.12.318.

Park, D.H., Joe, Y.H., Piri, A., An, S., Hwang, J., 2020. Determination of air filter anti-viral efficiency against an airborne infectious virus. J. Hazard Mater. 396, 122640. https://doi.org/10.1016/j.jhazmat.2020.122640.

Payne, S., 2017. Introduction to DNA viruses. Viruses. https://doi.org/10.1016/b978-0-12-803109-4.00028-3, 231–6.
Payne, S., 2017. Introduction to RNA viruses. Viruses 97–105. https://doi.org/10.1016/b978-0-12-803109-4.00010-6.
Quach, Q.H., Ang, S.K., Chu, J.H.J., Kah, J.C.Y., 2018. Size-dependent neutralizing activity of gold nanoparticle-based subunit vaccine against dengue virus. Acta Biomater. 78, 224–235. https://doi.org/10.1016/j.actbio.2018.08.011.
Ramadan, M.A., Shawkey, A.E., Rabeh, M.A., Abdellatif, A.O., 2020. Promising antimicrobial activities of oil and silver nanoparticles obtained from Melaleuca alternifolia leaves against selected skin-infecting pathogens. J. Herb. Med. 20, 100289. https://doi.org/10.1016/j.hermed.2019.100289.
Ratan, Z.A., Mashrur, F.R., Chhoan, A.P., Shahriar, S.M., Haidere, M.F., Runa, N.J., et al., 2021. Silver nanoparticles as potential antiviral agents. Pharmaceutics 13, 2034. https://doi.org/10.3390/pharmaceutics13122034.
Rodriguez-Izquierdo, I., Serramia, M., Gomez, R., De La Mata, F., Bullido, M., Muñoz-Fernández, M., 2020. Gold nanoparticles crossing blood-brain barrier prevent HSV-1 infection and reduce herpes associated amyloid-βsecretion. J. Clin. Med. 9, 155. https://doi.org/10.3390/jcm9010155.
Rónavári, A., Kovács, D., Igaz, N., Vágvölgyi, C., Boros, I.M., Kónya, Z., et al., 2017. Biological activity of green-synthesized silver nanoparticles depends on the applied natural extracts: a comprehensive study. Int. J. Nanomed. 12, 871–883. https://doi.org/10.2147/IJN.S122842.
Seino, S., Imoto, Y., Kosaka, T., Nishida, T., Nakagawa, T., Yamamoto, T.A., 2016. Antiviral activity of silver nanoparticles immobilized onto textile fabrics synthesized by radiochemical process. MRS Adv. 1, 705–710. https://doi.org/10.1557/adv.2016.43.
Sekimukai, H., Iwata-Yoshikawa, N., Fukushi, S., Tani, H., Kataoka, M., Suzuki, T., et al., 2020. Gold nanoparticle-adjuvanted S protein induces a strong antigen-specific IgG response against severe acute respiratory syndrome-related coronavirus infection, but fails to induce protective antibodies and limit eosinophilic infiltration in lungs. Microbiol. Immunol. 64, 33–51. https://doi.org/10.1111/1348-0421.12754.
Shady, N.H., Khattab, A.R., Ahmed, S., Liu, M., Quinn, R.J., Fouad, M.A., et al., 2020. Hepatitis c virus ns3 protease and helicase inhibitors from red sea sponge (Amphimedon) species in green synthesized silver nanoparticles assisted by in silico modeling and metabolic profiling. Int. J. Nanomed. 15, 3377–3389. https://doi.org/10.2147/IJN.S233766.
Sharma, R.K., Cwiklinski, K., Aalinkeel, R., Reynolds, J.L., Sykes, D.E., Quaye, E., et al., 2017. Immunomodulatory activities of curcumin-stabilized silver nanoparticles: efficacy as an antiretroviral therapeutic. Immunol. Invest. 46, 833–846. https://doi.org/10.1080/08820139.2017.1371908.
Sharma, V., Kaushik, S., Pandit, P., Dhull, D., Yadav, J.P., Kaushik, S., 2019. Green synthesis of silver nanoparticles from medicinal plants and evaluation of their antiviral potential against chikungunya virus. Appl. Microbiol. Biotechnol. 103, 881–891. https://doi.org/10.1007/s00253-018-9488-1.
Shimabuku, Q.L., Arakawa, F.S., Fernandes Silva, M., Ferri Coldebella, P., Ueda-Nakamura, T., Fagundes-Klen, M.R., et al., 2017. Water treatment with exceptional virus inactivation using activated carbon modified with silver (Ag) and copper oxide (CuO) nanoparticles. Environ Technol (United Kingdom) 38, 2058–2069. https://doi.org/10.1080/09593330.2016.1245361.
Singh, L., Kruger, H.G., Maguire, G.E.M., Govender, T., Parboosing, R., 2019. Development and evaluation of peptide-functionalized gold nanoparticles for HIV integrase inhibition. Int. J. Pept. Res. Ther. 25, 311–322. https://doi.org/10.1007/s10989-018-9673-1.
Soliman, M.G., Mohamed, A.F., Sayed, RA El, Elqasem, A.A.A., 2017. Immunohistochemical and histological changes in the spleen induced by gold nanoparticles as alternative adjuvant against rift valley fever virus. Eur. J. Biomed. Pharm. Sci. 4, 537–542.
Sreekanth, T.V.M., Nagajyothi, P.C., Muthuraman, P., Enkhtaivan, G., Vattikuti, S.V.P., Tettey, C.O., et al., 2018. Ultra-sonication-assisted silver nanoparticles using Panax ginseng root extract and their anti-cancer and antiviral activities. J. Photochem. Photobiol. B Biol. 188, 6–11. https://doi.org/10.1016/j.jphotobiol.2018.08.013.
Stone, J.W., Thornburg, N.J., Blum, D.L., Kuhn, S.J., Wright, D.W., Crowe, J.E., 2013. Gold nanorod vaccine for respiratory syncytial virus. Nanotechnology 24. https://doi.org/10.1088/0957-4484/24/29/295102.
Sujitha, V., Murugan, K., Paulpandi, M., Panneerselvam, C., Suresh, U., Roni, M., et al., 2015. Green-synthesized silver nanoparticles as a novel control tool against dengue virus (DEN-2) and its primary vector Aedes aegypti. Parasitol. Res. 114, 3315–3325. https://doi.org/10.1007/s00436-015-4556-2.
Talebian, S., Wallace, G.G., Schroeder, A., Stellacci, F., Conde, J., 2020. Nanotechnology-based disinfectants and sensors for SARS-CoV-2. Nat. Nanotechnol. 15, 618–621. https://doi.org/10.1038/s41565-020-0751-0.
Tamil Selvan, S., Balasubramani, G., Narayanasamy, S., Ramamurthy, D., 2019. Evaluation of multitudinous potentials of photosynthetic microalga, Neochloris aquatica RDS02 derived silver nanoparticles. Smart Sci. 7, 116–129. https://doi.org/10.1080/23080477.2018.1491743.
Tao, W., Hurst, B.L., Shakya, A.K., Uddin, M.J., Ingrole, R.S.J., Hernandez-Sanabria, M., et al., 2017. Consensus M2e peptide conjugated to gold nanoparticles confers protection against H1N1, H3N2 and H5N1 influenza A viruses. Antiviral Res. 141, 62–72. https://doi.org/10.1016/j.antiviral.2017.01.021.
Teng, Z., Sun, S., Chen, H., Huang, J., Du, P., Dong, H., et al., 2018. Golden-star nanoparticles as adjuvant effectively promotes immune response to foot-and-mouth disease virus-like particles vaccine. Vaccine 36, 6752–6760. https://doi.org/10.1016/j.vaccine.2018.09.030.
Tram, D.T.N., Wang, H., Sugiarto, S., Li, T., Ang, W.H., Lee, C., et al., 2016. Advances in nanomaterials and their applications in point of care (POC) devices for the diagnosis of infectious diseases. Biotechnol. Adv. 34, 1275–1288. https://doi.org/10.1016/j.biotechadv.2016.09.003.
Vijilvani, C., Bindhu, M.R., Princy, F.C., AlSalhi, M.S., Sabitha, S., Saravanakumar, K., et al., 2019. Antimicrobial and catalytic activities of biosynthesized gold, silver and palladium nanoparticles from Solanum nigurum leaves. J. Photochem. Photobiol. B Biol. 111713. https://doi.org/10.1016/j.jphotobiol.2019.111713.
Vo, T., Nguyen, T.T., Huynh, T.T., Vo, T.T., Nguyen, T.T., Nguyen, D., et al., 2019. Biosynthesis of silver and gold nanoparticles using aqueous extract from Crinum latifolium leaf and their applications forward antibacterial effect and wastewater treatment. J. Nanomater. 2019, 1–14. https://doi.org/10.1155/2019/8385935.
Weiss, C., Carriere, M., Fusco, L., Fusco, L., Capua, I., Regla-Nava, J.A., et al., 2020. Toward nanotechnology-enabled approaches against the COVID-19 pandemic. ACS Nano 14, 6383–6406. https://doi.org/10.1021/acsnano.0c03697.
Wu, J., Zhao, M., Wang, Y., Wang, Y., Zhu, H., Zhao, S., et al., 2017. N - (3-hydroxymethyl- β -carboline-1-yl-ethyl- 2-yl) - l -Phe : development toward a nanoscaled antitumor drug capable of treating complicated thrombosis and inflammation. Drug Des. Dev. Ther. 11, 225–239.
Yaqoob, S.B., Adnan, R., Muhammad, R., Khan, R., 2020. Gold , silver , and palladium nanoparticles : a chemical tool for biomedical applications. Front. Chem. 8, 1–15. https://doi.org/10.3389/fchem.2020.00376.
Zazo, H., Colino, C.I., Warzecha, K.T., Hoss, M., Gbureck, U., Trautwein, C., et al., 2017. Gold nanocarriers for macrophage-targeted therapy of human immunodeficiency virus. Macromol. Biosci. 17, 1–6. https://doi.org/10.1002/mabi.201600359.
Zeedan, G.S.G., Abd El-Razik, K.A., Allam, A.M., Abdalhamed, A.M., Abou Zeina, H.A., 2020. Evaluations of potential antiviral effects of green zinc oxide and silver nanoparticles against bovine herpesvirus-1. Adv. Anim. Vet. Sci. 8, 433–443. https://doi.org/10.17582/journal.aavs/2020/8.4.433.443.
Zhang, R., Lin, Z., Lui, V.C., Wong, K.K., Tam, P.K., Lee, P., et al., 2017. Silver nanoparticle treatment ameliorates biliary atresia syndrome in rhesus rotavirus inoculated mice. Nanomed. Nanotechnol. Biol. Med. 13, 1041–1050. https://doi.org/10.1016/j.nano.2016.11.013.